Microfluid Nanofluid (2010) 9:1185–1214
DOI 10.1007/s10404-010-0640-1

RESEARCH PAPER

Nanotubes-/nanowires-based, microfluidic-integrated transistors for detecting biomolecules

J. N. Tey · I. P. M. Wijaya · J. Wei · I. Rodriguez · S. G. Mhaisalkar

Received: 4 February 2010 / Accepted: 19 April 2010 / Published online: 3 June 2010

Abstract Nanotubes and nanowires have sparked considerable interest in biosensing applications due to their exceptional charge transport properties and size compatibility with biomolecules. Among the various biosensing methodologies incorporating these nanostructured materials in their sensing platforms, liquid-gated field-effect transistors (LGFETs)-based device configurations outperform the conventional electrochemical measurements by their ability in providing label free, direct electronic readout, and real-time detection. Together with integration of a microfluidic channel into the device architecture, nanotube- or nanowires-based LGFET biosensor have demonstrated promising potential toward the realization of truly field-deployable self-contained lab-on-chip devices, which aim to complement the existing lab-based methodologies. This review addresses the recent advances in microfluidic-integrated carbon nanotubes and inorganic nanowires-based LGFET biosensors inclusive of nanomaterials growth, device fabrication, sensing mechanisms, and interaction of biomolecules with nanotubes and nanowires. Design considerations, factors affecting sensing performance and sensitivity, amplification and multiplexing strategies are also detailed to provide a comprehensive understanding of present biosensors and future sensor systems development.

Keywords Biosensor · Carbon nanotubes · Nanowires · Label-free detection · Field-effect transistor

1 Introduction

One-dimensional nanostructures such as carbon nanotubes (CNTs) and nanowires (NWs) have been envisaged as ideal building blocks for biosensor development due to their size similarity and biocompatibility with a host of biomolecules. Their extremely high surface-to-volume ratio results in most of the constituent atoms residing on the surface of the nanostructure, which renders even the slightest disturbance from their proxy surrounding sufficient to alter their electrical properties (Lacerda et al. 2006, 2007; Polizu et al. 2006; Popov et al. 2007). As compared to their zero- or two-dimensional counterparts, one-dimensional nanosystems such as nanotubes and nanowires offer a major advantage in that its length scale that extends into micrometers offers a facile route for interfacing to the macro world. In the case of zero-dimensional nanosystems, such as nanoparticles and quantum dots, this interfacing becomes a challenge due to complexities in inter-particle charge transport. On the other hand, two-dimensional nanosystems like graphene and flat nanocrystals, exhibit tensor (non-scalar) nature of the conductivities, which result in anisotropy in electrical properties. Furthermore, any local electrostatic disturbance may not always be detected because of the large conducting surfaces charges may naturally circumvent such areas choosing the path of

First two authors contributed equally to this work.

J. N. Tey · J. Wei
Singapore Institute of Manufacturing Technology, 71 Nanyang Drive, Singapore 638075, Singapore

I. P. M. Wijaya · I. Rodriguez
Institute of Materials Research and Engineering, 3 Research Link, Singapore 117602, Singapore

J. N. Tey · I. P. M. Wijaya · S. G. Mhaisalkar (✉)
School of Materials Science and Engineering, Nanyang Technological University, Block N4.1, Nanyang Avenue, Singapore 639798, Singapore
e-mail: Subodh@ntu.edu.sg

least resistance. Both zero-dimensional and two-dimensional nanosystems thus present challenges from interfacing and device optimization perspective.

Different device architectures have been designed over the last decades to utilize these nanostructured materials as sensing elements to detect biomolecular interactions. In general, detection methods in sensing configurations incorporating CNTs and NWs include: (1) fluorescence (Hazani et al. 2003; Cherukuri et al. 2006), (2) electrochemistry (Gooding et al. 2003; Kim et al. 2007b; Diao et al. 2002; Huang et al. 2009), and (3) transistor-based electrical sensing (Heller et al. 2008; Bradley et al. 2004, 2005; Jeon et al. 2006; Guo et al. 2003; Star et al. 2003; Gui et al. 2006; Chen et al. 2004). Classical detection techniques such as enzyme-linked immunosorbent assay (ELISA), cyclic voltammetry, amperometry, potentiometric, and electrochemical impedance spectroscopy have been reported to display significant improvement upon incorporating CNTs into the measurement setup, such as blending of CNTs into the electrodes (Gong et al. 2005; Yun et al. 2007; Panini et al. 2008) or using them as labels for signal amplification (Wang et al. 2004; Yu et al. 2006). Nonetheless, these techniques typically suffer a few drawbacks: (1) extra processing steps are required to introduce a fluorescence or electrochemical tag to the system in order to probe the biomolecular interaction, (2) sensing is not performed in real-time, and (3) they are usually not adaptable for on-site analysis.

To address these challenges, a new alternative to detect these biomolecular interaction in label-free fashion have recently been proposed, utilizing semiconducting CNT and NW as the semiconducting channel in field-effect transistors (FETs) (Kim et al. 2007b). While the history of semiconductors and the first reported semiconductor FET dates back for more than a century (Braun 1874; Bardeen and Brattain 1948; Kahng and Atalla 1960), the advancement of CNTs and NWs dates back to merely two decades (Iijima 1991; Hu et al. 1999); with their potential for sensing applications in transistor configuration reported only as recently as 2000 (Kong et al. 2000; Cui et al. 2001). Specifically, two approaches have been reported: dry-state sensing (Gui et al. 2006; Star et al. 2006) and liquid-gated transistor (LGFET) (Cui and Lieber 2001; Rosenblatt et al. 2002) measurement, in which the latter offers an added benefit in permitting real-time detection of biomolecular interactions in aqueous media, the native environment for most biomolecules. The motivation toward transistor-based biosensors is not to replace, but rather complement established high sensitivity analytical methods such as ELISA, to address needs for point-of-care diagnostics and on-site sample analysis.

While FET-based biosensors have demonstrated promising detection limits, greater considerations for device miniaturization, real-time sensing and portability are required toward the realization of truly field-deployable self-contained lab-on-chip devices. The integration of microfluidic channel into the transistor architecture was first demonstrated on the NW-LGFET-based biosensing study (Cui et al. 2001), and much later after that for CNT–LGFET (Larrimore et al. 2006). Even though the starting point for NWs research effort took place much later than the CNTs, the development of the former and its process integration for lab-on-chip capability has been particularly rapid. This rapid development in the NW–LGFET platforms was facilitated by the mature body of knowledge gleaned in the field of silicon microelectronics. The incorporation of microfluidic channels into the sensor architecture represents a critical innovation in the realization of lab-on-chip devices. Advantages include (1) significant reduction in analyte volume requirement; (2) reduced incubation time due to shorter diffusion distances as a result of molecules being confined in the microchannel; (3) better control of molecular concentrations and interactions; and (4) ability to execute multiple complex reactions including lysis, amplification, mixing, filtration among others.

In this review article, a brief survey of the recent advances of microfluidic-integrated LGFET-based biosensors is addressed. While CNTs and NWs are different in their molecular structures, growth, and fabrication processes, they share operational similarities when incorporated in FET-based biosensors. The objective of this review is to present an overview of the ongoing biosensing activities with microfluidic-integrated LGFET devices incorporating CNTs or NWs. General principles are explained in most part without making distinctions between CNTs and NWs. However, comments and comparisons between CNTs and NWs are made when required to elaborate their pros and cons, as well as to highlight parametric and process control differences between the two platforms.

The scope of this review includes aspects such as overview of the molecular structure of CNTs and NWs, the working principles and sensing mechanisms of LGFETs, as well as device assembly and fabrication. In addition, factors influencing the sensitivity of the measurement, potential techniques for signal amplification, and examples of LGFET-based biodetection of proteins, enzymes, and oligonucleotides will be covered. Due to the diversified nature of CNT-based sensing platforms and a variety of semiconducting NWs-based FET architectures (Jeon et al. 2006; Zhang et al. 2008a; Curreli et al. 2005; Patolsky et al. 2006b; Sun et al. 2010; Baker et al. 2002), it would be impractical to attempt a broad discussion on the field. Our discussion is therefore confined to the most promising nanomaterials and architectures for this application, single-

walled CNT (SWCNT) and silicon nanowire (SiNW)-based LGFETs. Throughout this review, general terms such as CNT and NW will refer to SWCNT and SiNW, unless specified otherwise.

2 Working principles of liquid-gated field-effect transistor-based biosensors

2.1 Molecular structure and electrical properties of CNTs and NWs

The CNTs and NWs are similar in that both share most of the characteristics of one-dimensional systems, such as quantum confinement at circumferential and radial directions, increased band gap as their cross-sectional diameter decreases, etc. However, the two nanosystems are also different in many ways depending on the arrangement of atoms.

CNTs belong to a class of carbonaceous nanomaterials in which a unique surface arrangement of carbon atoms coupled with one-dimensional quantum confinement gives rise to exceptional electronic, thermal, and mechanical properties. Numerous applications of these materials in molecular electronics, circuits and interconnects, field emission, actuators, energy harvesting and storage, high strength composites, biomedical diagnostics, and drug delivery (Dekker 1999; Kreupl et al. 2002; Endo et al. 2008) are currently being aggressively pursued. The versatility of nanotubes stems from their unique characteristics, including extremely large aspect ratios, high surface-to-volume ratios, infinitely conjugated sp^2 hybridized network of carbon atoms, impressive strength-to-weight ratios, and excellent chemical stability.

From a molecular structure perspective, the nanotubes are tubular analogs of graphene, and may be divided into single-walled carbon nanotubes (SWCNTs) and multi-walled carbon nanotubes (MWCNTs), depending on the number of graphene sheet(s) that form the structures (Anantram and Leonard 2006). SWCNTs comprise single graphene sheet rolled into a cylindrical architecture with dimensions typically in the order of 1–2 nm in diameter and several micro-meters in length. In contrast, MWCNTs can be visualized as multiple graphene sheets rolled together into concentric nano-sized cylinders with layer to layer spacing of 0.3–0.4 nm, diameters of 10–100 nm and lengths of several micro-meters (Baughman et al. 2002).

The different atomic arrangement of the two nanotubes sub-species manifests itself in their electronic properties. The SWCNT, for example, is well-known for its unique electronic properties in that it can behave like either semiconductors, or metals, depending on the specific arrangement of the carbon atoms in the SWCNT. In contrast, MWCNTs tend to behave more like metals. These different electronic properties have led to divergent applications of semiconducting SWCNTs as transistors for future microelectronic and sensing devices (Jo et al. 2007; Kim et al. 2007b; Anantram and Leonard 2006; Bradley et al. 2004; Star et al. 2003) and metallic MWCNTs as microelectrodes in electrochemical sensors (Panini et al. 2008; Viswanathan et al. 2009).

The unique electronic properties of the SWCNTs, which can display either semiconducting or metallic properties, are product of a phenomenon observed only in the nanoscale realm: quantum confinement. Briefly, the quantum confinement effect takes place when the wavelength of the charge carriers is similar to the physical environment in which they reside. The wave continuity requirement dictates that the charge carriers cannot assume all wavelength values in such confined environments. This restriction results in the charge carriers to assume only certain portions of the energy–momentum diagram. Graphically, this discontinuity can be depicted as slicing planes which cut only certain portions of an otherwise continuous energy–momentum diagram, as shown in Fig. 1a (Dresselhaus et al. 2005). Hence, from this graph, it can be envisaged that the rolling direction of the CNTs would dictate the profile of the energy–momentum diagram. Therefore, within a family of CNTs, there would be those that show a band gap, rendering them semiconducting, and those that are metallic.

Similar to their nanotube counterparts, one-dimensional nanowires display differing properties as influenced by the atomic constituents, geometry, dimensions, presence of dopants, point defects, etc. However, unlike their nanotube counterparts, the parameters to synthesize the nanowires are more controllable, making the batch-to-batch properties of these nanowires more uniform (Hu et al. 1999). In addition, analog electrical properties are also displayed by the nanowires, as shown in Fig. 1b (Yao et al. 2008). Similar to the CNTs, the energy–momentum diagram of the NWs also suffers from quantum-confinement effect. The extent of this quantum-confinement effect is different at the various points in the energy–momentum diagram. Indeed, this variation to sensitivity toward the quantum-confinement effect makes SiNWs very different from their bulk Si counterparts in that the former typically is a direct band gap semiconductor, hence rendering it a suitable material relevant to photonic applications.

The similarity in the energy–momentum diagram as displayed by both the NWs and the CNTs makes these two one-dimensional nanosystems amenable to be brought into the same LGFET platform. Specifically, the NWs and the CNTs can be connected to source–drain electrodes at both extremes to make a simple Schottky transistor typical of LGFETs. Furthermore, the size similarity between most

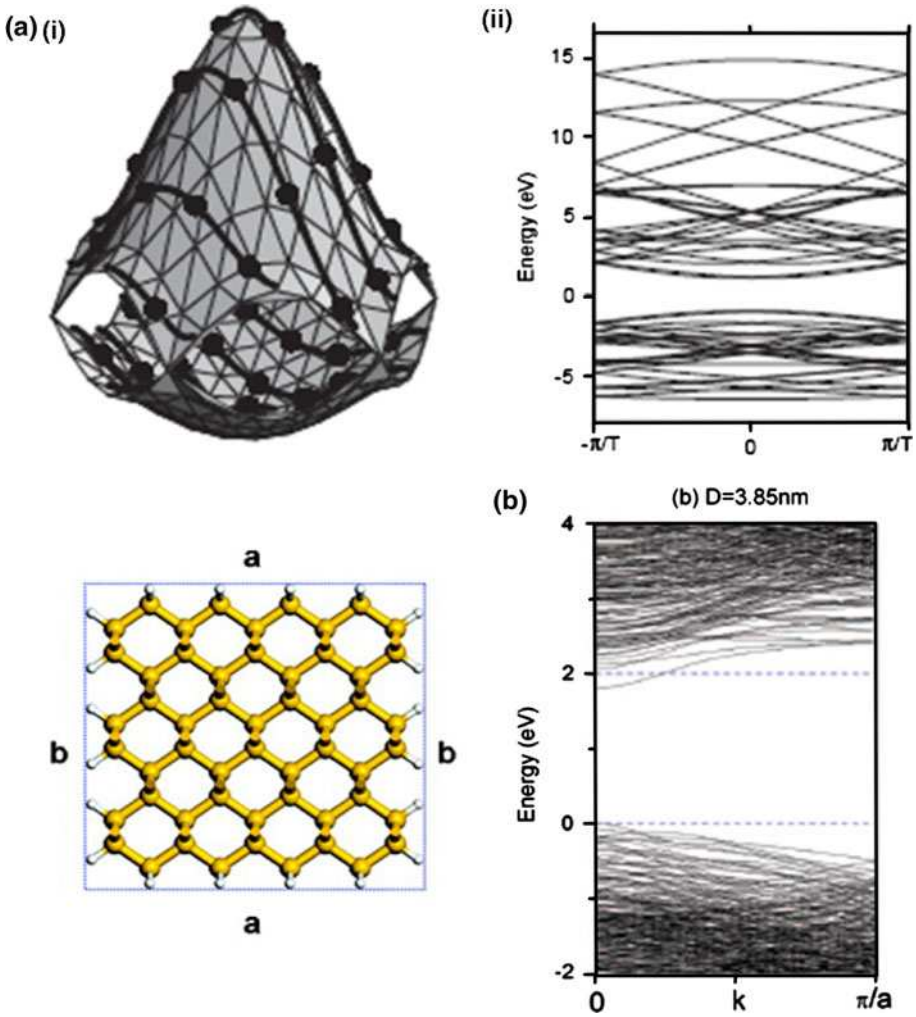

Fig. 1 **a** *E–k* diagram showing the energy quantization which appears as slicing planes along the rolling directions in (*i*) and its cross-sectional view in (*ii*). **b** *E–k* diagram for SiNW having a rectangular cross section with diameter of 3.85 nm. Image **a** adapted from Dresselhaus et al. (2005). Image **b** adapted with permission from Yao et al. (2008). Copyright (2008) American Chemical Society

biomolecules with the NWs and the CNTs makes them the preferred choice for development of real-time label-free biosensors.

To conclude, the electrical properties of SWCNTs vary according to their diameter and chiral distribution (Anantram and Leonard 2006; LeMieux et al. 2008), which are difficult to control during their growth processes and challenges their viability in large-scale commercial applications. Unlike CNTs, the prime advantage of SiNWs is that their electrical properties can be controlled by classical doping practices, commonly employed in the microelectronics field. Hence, the vast knowledge from the semiconductor industry can be transferred and applied to the fabrication, doping, and surface chemical modification of these nanowires (Cui et al. 2000; Pui et al. 2009; Zhang et al. 2008b). In addition, distinct chemical composition, structure, size, and morphology can be well controlled through the growth process (Lu and Lieber 2006). The highly reproducible electronic properties and high yield production has made SiNW a promising nanomaterial for future large-scale integrated systems and potential bioapplications, including the field of environmental sensing and medical diagnostics.

2.2 Working principles: LGFET versus dry-state FET

Typically, a CNT or NW–FET comprises CNTs or NWs as the semiconducting channel that is capacitively coupled to a gate electrode through a dielectric medium and flanked by metal source–drain electrodes to provide electrical connectivity (Fig. 2a). Voltage applied to the gate electrode (V_G) modulates the charge carrier concentration induced in the semiconducting channel at the dielectric–semiconductor interface, hence modulating the drain–source conductance. Considering a p-type FET, an application of negative V_G bias leads to the accumulation of hole carriers, and hence current flows from the source to the drain electrode upon applying a source–drain Voltage (V_{DS}) across the channel. A positive V_G bias will lead to the depletion of carriers at the interface, restricting the current flow.

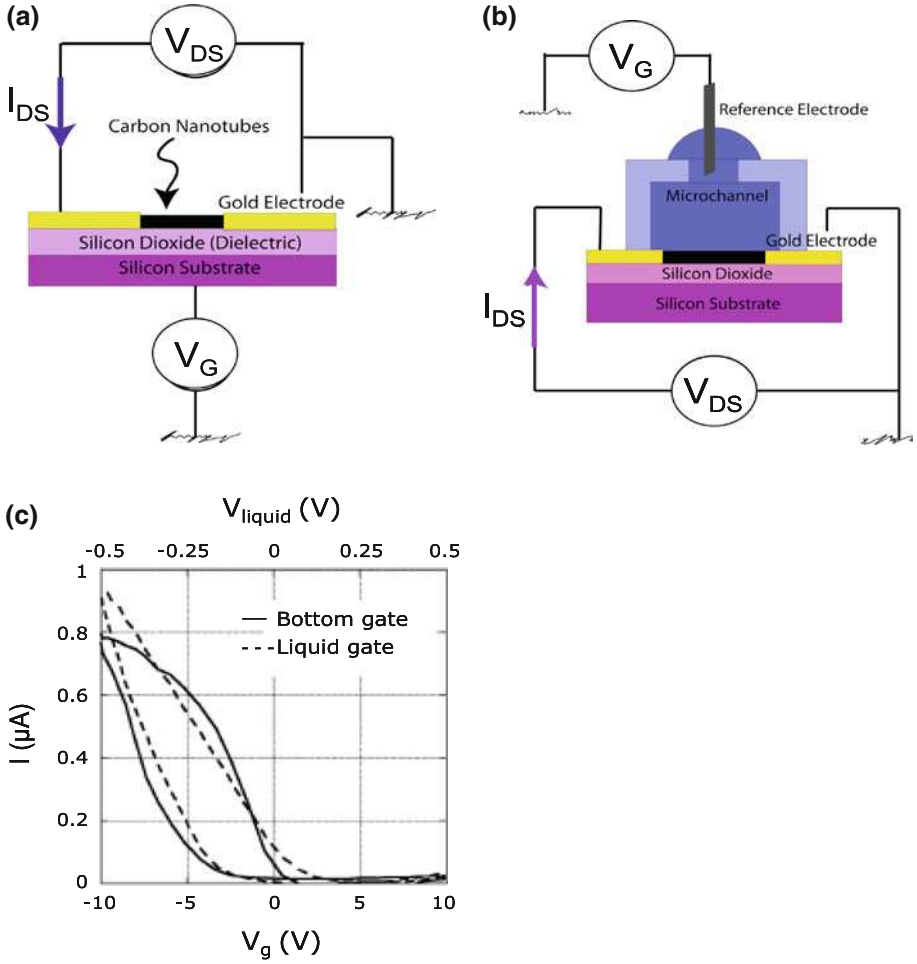

Fig. 2 **a** Dry-state CNT–FET in bottom gate configuration. **b** Liquid state CNT–FET in top electrolyte gate configuration. **c** Comparison of CNT–FET transfer characteristic (I_D–V_G) in air, using the bottom gate (*solid line*), and in water, using the liquid gate (*dotted line*). Note the different x scales for the bottom gate and the liquid gate. Image **c** adapted with permission from Bradley et al. (2004). Copyright (2004) American Chemical Society

The dielectric layer, typically composed of a solid dielectric film in a dry-state FET, is replaced by an aqueous electrolyte solution in liquid-gated FETs (Fig. 2b). A gate bias is applied directly to the electrolyte solution to modulate the surface carrier concentration of the semiconducting channel, thereby modulating the channel conductance. One important advantage of employing the LGFET configuration in biosensors is that the aqueous environment is highly compatible with biomolecules. In addition, the V_G range required to modulate the channel conductance (hereafter referred to as V_G window) is significantly reduced, with much smaller hysteresis in the electrical measurement.

The operation of LGFET as biosensors is sometimes confused with ion-selective field-effect transistors (ISFET) (Jamasb et al. 1998). In the latter, the presence of target analyte ions in solution is captured by a suitable probe dielectric material. Such biomolecular interactions can only influence a thin region near the surface of a planar device, limiting the sensitivity of the device (Lieber and Wang 2007). In LGFET operation, when a bioanalyte interacts with its probe molecule close to the surface of the CNTs/NWs, it leads to depletion or accumulation of charge carriers throughout the nanostructures, resulting in higher sensitivity.

The gate voltage required to modulate the semiconducting channel of CNT or NW–FET is governed by the total gate channel capacitance in Eq. 1, which is composed of two components: gate capacitance (C_G) and quantum capacitance (C_Q).

$$C_T = \left(\frac{1}{C_G} + \frac{1}{C_Q}\right)^{-1} \quad (1)$$

C_Q originates from the small size of the nano-structures. The minute size of the nanostructures results in a limited number of the energy states available for the carriers to occupy. Any addition of charge carriers to the nanostructures would require an application of external voltage to modulate the energy level to the next available state. Hence, the requirement of voltage to add/subtract charge carriers from the nanostructures is represented as $C = \delta Q/\delta V$ and $C_Q = e^2\, g(E)$.

For LGFETs, C_G is the double-layer capacitance (C_{DL}) resulting from the formation of electrical charge layers at

both the semiconducting nanostructure–solution interface and the solution–gate electrode interface (Rosenblatt et al. 2002; Lu et al. 2006). The high dielectric constant of the aqueous media ($\varepsilon_r \sim 78$) and thin electrical double layer in LGFET results in C_G of a liquid-gated FET ($C_{GL} \sim 7 \times 10^{-9}$ F/m) (Rosenblatt et al. 2002), being approximately two orders of magnitude higher than that of the dry-state FET, (C_{BG}), which uses silicon dioxide ($\varepsilon_r \sim 3.9$) as the dielectric layer (Martel et al. 1998), and around one order of magnitude larger than C_Q of SWCNT/NW. Therefore, C_T in a back-gated dry-state SWCNT/NW–FET is constrained by the oxide dielectric while C_T in liquid-gated SWCNT/NW–FET is dominated by the C_Q of SWCNT or NW, yielding a 10-fold improvement in capacitance.

This improved performance of the LGFET is evident in the I_D versus V_G ("transfer") curves for a dry-state FET and LGFET (Fig. 2c). In order to generate equivalent current outputs, the dry-state FETs need to operate at significantly higher voltages ($10 \geq V_G \geq -10$ V) compared with the LGFETs which may operate at less than |0.5| V (Gruner 2006; Bradley et al. 2004).

Another significant advantage of LGFETs over dry-state FET biosensing is the ability for real-time detection. Examples of reported dry-state measurements include direct detection of streptavidin (Bradley et al. 2004) and bacteriorhodopsin (Bradley et al. 2005), as well as capture-target analyte detection for biotin/streptavidin conjugate (Star et al. 2003) and DNA hybridization (Star et al. 2006). In these studies, transfer characteristics of the CNT or NW transistor before and after bioanalytes exposure are compared. To perform the measurements, the bare transistor performance is first recorded prior to the incubation of analytes. Upon completing the incubation process, the device is rinsed with copious amounts of buffer solution to remove the unbound analytes, blown dry, and post-binding electrical measurement is executed. Repeat incubation, rinsing, drying, and measurement steps have to be carried out to record the change in I_DV_G in every step (Fig. 3a). Multiple incubations, if required, expose the nanostructured FETs to multiple processing steps and have the potential of introducing inconsistencies and compromise the quality of the sensing data.

In liquid-gated configurations, handling of respective processing steps can be simplified by conducting all the incubation and washing steps in situ by flowing different solutions into a micro-fluidic channel. In this scenario, dynamic information of the interaction can be studied without interrupting the electrical measurement, and series of transfer curves, taken at short-time intervals, yield quasi-kinetic data that may be analyzed in similar fashion to that of dry-state measurements. Figure 3a shows the transfer curves of a LGFET in an interrupted measurement and Fig. 3b shows a kinetic measurement where all electrode biases are held constant and the drain current with respect to time is measured. In both figures, trace 1 is the bare device transistor characteristic, while traces 2–4 show the electrical characteristics after repeated steps of incubation and rinsing.

2.3 Sensing mechanisms in LGFET-based biosensors

The change in conductance of CNT–LGFET in response to biomolecule interactions have been attributed to several competing mechanisms such as electrostatic gating effect (Bradley et al. 2005; Boussaad et al. 2003), charge transfer (Bradley et al. 2004; Star et al. 2003, 2006), and Schottky barrier effect due to work function modulation (Chen et al. 2004; Tang et al. 2006). Each of these hypotheses is well supported by experimental data and the sensing mechanism continues to be an area of active research. A recent comprehensive theoretical and experimental study reported on four possible mechanisms operational in a biomolecule-nanostructure interaction (Heller et al. 2008): (1) electrostatic gating, (2) Schottky barrier, (3) mobility, and (4) capacitance modulation; each of which exhibit a particular characteristic change in

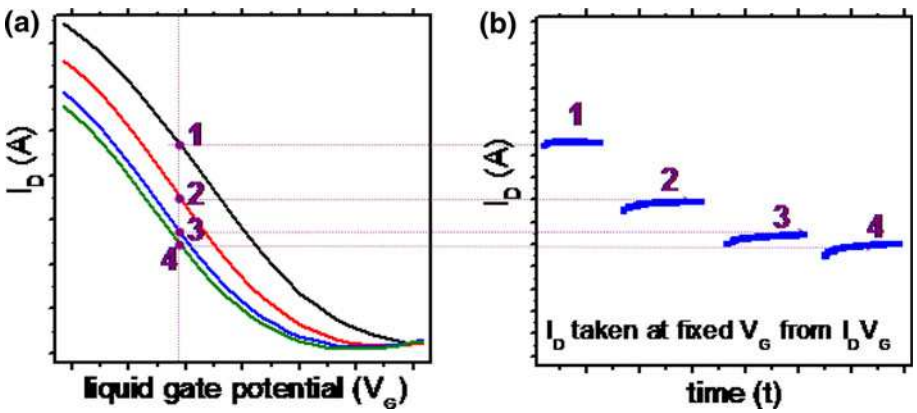

Fig. 3 **a** Transfer characteristic curves of a CNT–FET measured at every experiment step, through offline measurements of current over a sweeping gate bias, to observe the change in transistor response as a result of biomolecule–CNT interaction. **b** Kinetic measurement to observe the real-time response throughout the entire sensing experiment, obtained at a fixed gate bias

the I_{DS}–V_G curve. For example, the electrostatic gating mechanism is generally correlated with a threshold voltage shift; Schottky barrier modulation is characterized by a decrease in I_{DS} at $V_G < 0$ and increase in I_{DS} at $V_G > 0$; and capacitance and mobility changes manifest themselves in a change in transconductance and decrease in I_{DS}, respectively (Fig. 4). Of these possible mechanisms, a series of studies have shown that the predominant sensing mechanism in LGFET comes from electrostatic gating (Curreli et al. 2008; Li et al. 2005; Maehashi et al. 2006; Tey et al. 2009; Wijaya et al. 2009) and/or Schottky barrier modulation (Gui et al. 2007; Byon and Choi 2006).

Such complications are absent in the development of NW transistors for biosensing applications (Hahm and Lieber 2004; Wang et al. 2005; Zheng et al. 2005), where electrostatic gating is accepted as the dominant factor in the conductance modulation. Schottky barrier modulation and change in metal work function at the interface do play a role in the experimentation, but their influences are usually eliminated by silicon nitride (Si_3N_4) passivation that covers all electrical contacts, exposing only the nanowires in the active sensing region (Gao et al. 2007; Zheng et al. 2005; Patolsky et al. 2004), to ensure the detection signal to be purely dependent on electrostatic gating modulation.

3 Devices: fabrication and factors influencing biosensing in microfluidic-integrated LGFET

3.1 Synthesis of nanotubes/nanowires

CNTs and NWs are generally produced by vapor–liquid–solid (VLS) process using metal nanoclusters as catalyst (Kolasinski 2006; Lu and Lieber 2006; Patolsky et al. 2006b). One unique advantage of this growth process is to allow the selective growth of CNTs or NWs on desired locations of the underlying substrate through catalyst patterning (Curreli et al. 2008). In this method, catalyst nanoparticles are first assembled and/or patterned on the substrate surface, and a stream of carrier gas containing the precursor molecules is introduced at elevated temperatures. The reaction between the precursors and catalyst nanoparticles decomposes and dissolves the molten catalyst, and precipitates the semiconductor out of the molten catalyst upon reaching the level of saturation, leading to the growth of CNTs/NWs from the nucleation sites. For nanowire synthesis, VLS has an additional advantage in that in situ doping is possible by mixing the dopant precursor with the carrier gas during the growth process (Curreli et al. 2008). Typical precursors for the synthesis of SWCNTs are ethanol (Huang et al. 2006), methane (Li et al. 2001; Kocabas et al. 2006), and ethylene (Kim et al. 2002); while silane

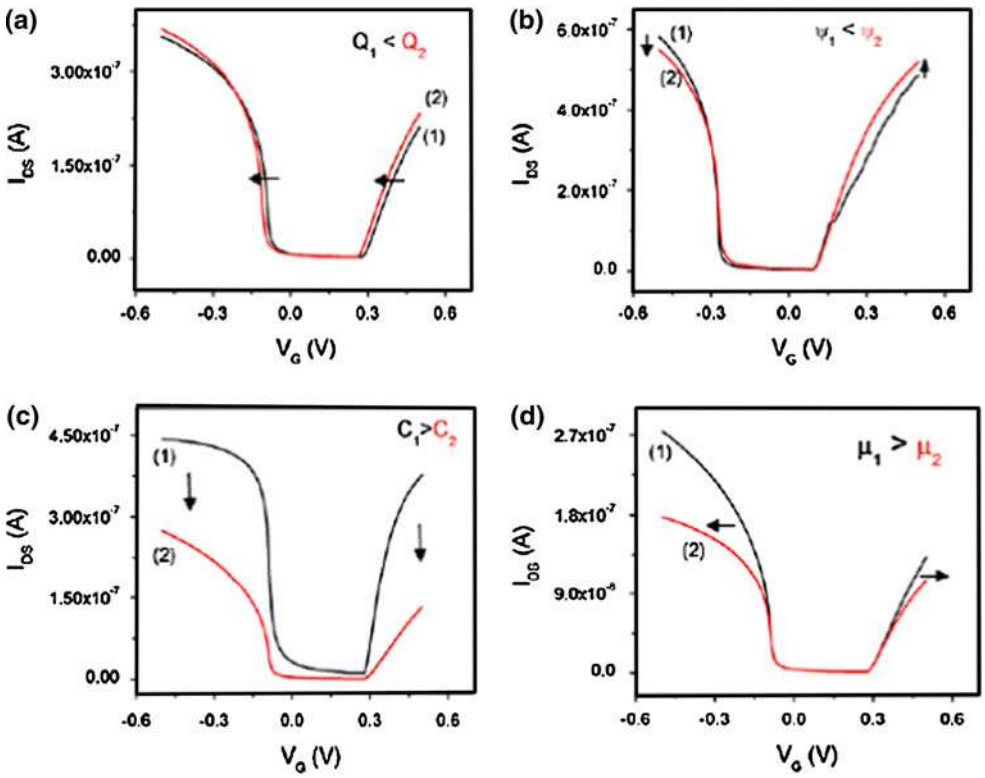

Fig. 4 Four possible scenarios whereby biomolecules can interact with SWCNT: **a** electrostatic gating modulation, **b** Schottky barrier modulation, **c** capacitance modulation, and **d** mobility modulation. Each possible mechanism displays a unique set of characteristic in the changes of the I_{DS}–V_G curves, allowing identification of the origin of the signal obtained. Simulation results as calculated from Landauer–Büttiker formalism, taking into account the effect of classical Drude's model (Wijaya et al. 2010a). Reproduced by permission of The Royal Society of Chemistry

gas and indium vapor are commonly used for the production of silicon and In_2O_3 nanowires, respectively (Li et al. 2003; Cui and Lieber 2001).

Subsequent to synthesis, the as grown CNTs/NWs usually do not assume the desired orientation, spatial, and dimensional specifications. Ultrasonication treatment is thus needed to first release the CNTs/NWs from the grown substrate into solution form, followed by subsequent appropriate assembly steps to re-deposit them onto the final substrate.

While standard micro-fabrication methodologies allow the growth of NWs with well controlled electrical properties through doping, post-processing is particularly important for SWCNTs, where randomized electronic properties are generated during the batch synthesis. Additional treatments are required to condition the CNTs by modifying or sorting the electrical properties prior to assembling them into suitable device structures. Critical processing steps include CNT purification (Liu et al. 1998; Dillon et al. 1999), separation of metallic and semiconducting tubes (Arnold et al. 2005; Strano et al. 2003; Stéphane et al. 2007), and functionalization (Hirsch and Vostrowsky 2005) of the tips and sidewalls prior to device integration.

3.2 Deposition of nanotubes/nanowires for the formation of FETs

Following the dispersion of CNTs/NWs into a solvent, they need to be assembled onto the substrate with controlled spatial and orientation distribution. Typical deposition methods employed include spin coating and/or drop-casting. Direct application of these techniques, however, produces a random network of CNTs/NWs without spatial and orientation control.

The spatial distribution of the assembly can be controlled by a "surface programmed assembly" (SPA) method, where the surface of the substrate is treated chemically with self-assembled monolayers (SAMs) whose patterns were used to direct the adsorption and alignment of CNTs/NWs on solid substrates from their suspension (Lee et al. 2009). For instance, trimethylsilyl and 3-aminopropyltriethoxysilane (APTES) treatments were employed on silicon oxide surface to create chemically functionalized templates with hydrophobicity and hydrophilicity control. Upon immersion of the treated substrates into the CNT dispersion, the nanotubes absorb preferentially on the APTES treated area (Fig. 5a) (Liu et al. 1999). Similar strategy using

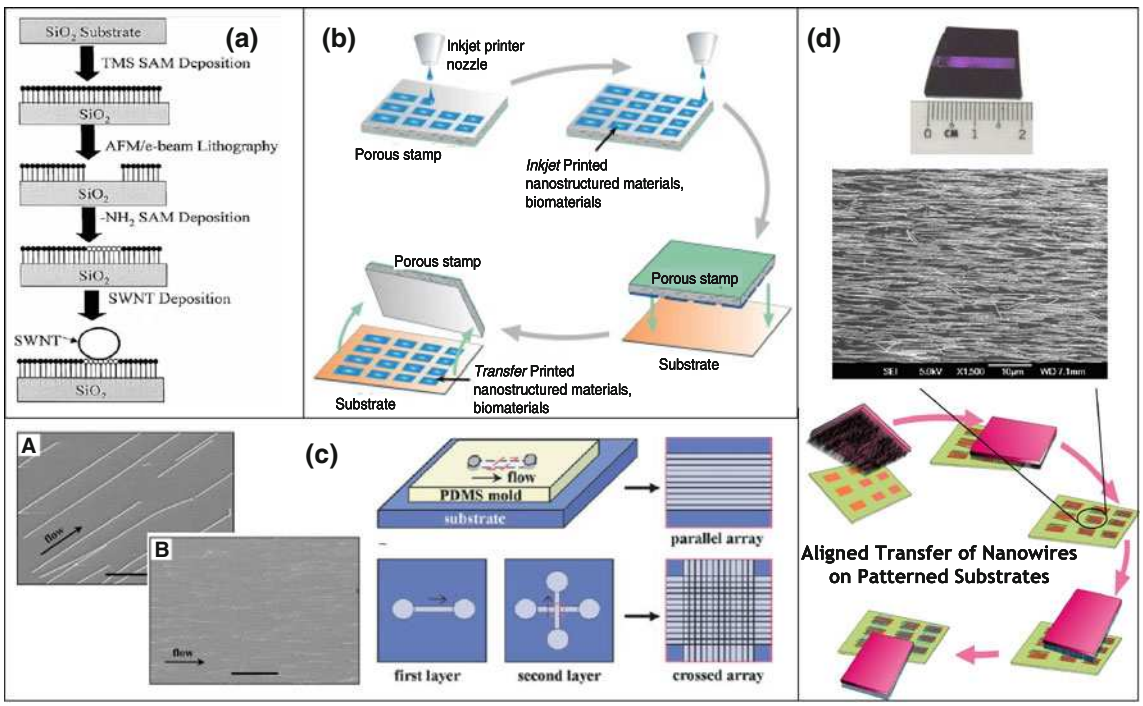

Fig. 5 **a** Schematic diagram showing the controlled deposition of CNTs on chemically functionalized lithographic patterns (Liu et al. 1999). Reprinted with permission from Elsevier. **b** Illustration of inkjet printing nanostructured materials followed by transfer printing to receiver substrate (Kumar et al. 2009). Reprinted with permission from Elsevier. **c** Schematic of fluidic channel structure of flow assembly to obtain flow guided aligned arrays of CNT/NW. Multiple crossed CNT/NW arrays can be achieved by changing the flow direction through layer by layer assembly process (Huang et al. 2001). Reprinted with permission from AAAS. **d** Schematic of the directional sliding method to achieve unidirectional NWs alignment. Multiple layers can be formed by subsequent sliding steps

different SAM layers was also applied on SiNW (Heo et al. 2008; Lee et al. 2006).

Alternatively, the nanotubes suspension can also be spin-coated directly onto a patterned PDMS stamp, followed by contacting the inked stamp onto a substrate with a higher surface energy than the PDMS (Meitl et al. 2004). This leads to efficient transfer of the tubes from the raised regions of the stamp. Besides the hydrophobic PDMS stamp, porous agarose gel was also reported for direct patterning of CNTs. The hydrophilic nature of the agarose stamp allows inkjet printing of solution-based CNT on the surface, followed by transfer printing to a base substrate to complete the formation of CNT pads without the need of photolithography (Kumar et al. 2009), as shown in Fig. 5b. Other examples of soft-lithography transfer methods include: (1) casting of a polymer film directly on silicon oxide surface with pre-grown tubes and pre-defined source-drain pads, followed by oxide etching to transfer the entire pattern to polymer films for plastic electronics fabrication (Bradley et al. 2003); (2) dry transfer method (Albrecht and Lyding 2003); and (3) contact or micro-contact printing (μCP) process through surface treatment of both PDMS stamp and receiver substrate (Park et al. 2007; Kim et al. 2007c; Kwang et al. 2009).

In the context of orientation control, partial alignment of CNTs can be achieved by spin coating the CNT suspensions directly on APTES treated surface (LeMieux et al. 2008). The resulting network structure possesses an alignment in radial direction from the center. Added advantage of this technique is the combination of tube separation, density and alignment in one step during device fabrication. Another common technique is through flow assembly (Park et al. 2006; Yan et al. 2006; Huang et al. 2001). The methodology involves the use of PDMS microfluidic channel to direct the flow of CNTs/NWs suspensions to achieve desired alignment and patterning; eliminating typical disadvantages in other processes, such as low deposition rate, non-scalability, the need for chemical modification on either the nanostructure or the substrates; or use of organic solvents that are incompatible with plastic device components (Fig. 5c). Other effective ways for alignment control include electric-field assisted assembly (Wijaya et al. 2008) and Langmuir–Blodgett (LB) technique (Lu and Lieber 2006; Kim et al. 2003). Hierarchically stacking nanowire building blocks into integrated arrays over large areas has been demonstrated with LB technique. The steps involve an uniaxial compression of the surfactant wrapped nanowire monolayers on an aqueous subphase into aligned nanowires with controlled spacing, followed by picking up and transfer of the compressed layer to a planar substrate (Whang et al. 2003). In addition to solution-based alignment processes, efforts in transferring perfectly aligned SWCNT network from quartz substrate to silicon oxide substrate has also been successful with PDMS transfer through the use of Au and polyimide/polyvinyl alcohol sacrificial layers (Kang et al. 2007a, b).

Besides the abovementioned methodologies, a transfer technique was developed to achieve alignment by transfer printing a "forest" of nanowires through directional sliding of the growth substrate onto a receiver substrate (Fan et al. 2008). The methodology can also be extended to achieve three-dimensional stacking nanowires array (Javey et al. 2007; Sun et al. 2010), as shown in Fig. 5d.

Alternatively, the nanowire fabrication and assembly can be integrated into one process flow through a top–down methodology (Gao et al. 2007; Stern et al. 2007a; Melosh et al. 2003). The SiNWs in this case are etched from a top layer made of single crystal silicon using oxidation and wet etching technique to define parallel aligned nanowires with identical dimension and properties. Despite the disadvantages of high cost incurred and slow production rate, top–down methods usually produce nanowires with high yields and predetermined orientation and position, facilitating integration into functional devices with good consistency (Curreli et al. 2008).

3.3 Design and fabrication of microfluidic-integrated FETs

Following the assembly of the nanowires and the nanotubes, source, drain, and gate electrodes are deposited to complete the transistor fabrication. A passivation layer is usually required to isolate areas such as interconnects and junction regions, to prevent bioanalytes adsorption onto these areas during the sensing measurement. Design considerations include the effect of channel width (W), channel length (L) which could affect the sensitivity of the sensor platform. Analytical calculation and finite element simulations highlight the importance of channel length to the response time of sensing (Sheehan and Whitman 2005; Nair and Alam 2007): the longer the electrical channel length, the shorter is the required incubation time owing to larger active region in which the biomolecules interact with the CNTs/NWs (Sheehan and Whitman 2005). However, device with long channel lengths will also degrade the sensitivity of the sensor due to the low W/L ratio (Nair and Alam 2007; Curreli et al. 2008). Hence, the FET architecture needs to be optimized to yield a balance between high sensitivity, reasonable incubation, and response time.

The microfluidic channel is introduced as the last step of the LGFET-based biosensors. The dimensions of the microchannel directly affect the fluid flow and hence the sensitivity of the biosensor. Typically, a PDMS microchannel is placed on top of the device to guide the solution flow to the active region where interaction and sensing

takes place (Stern et al. 2007a), as shown in Fig. 6a. This is the most commonly employed architecture for biosensing with CNT and NW–LGFET, and the underlying substrate is usually silicon. The established fabrication protocol allows the customization of different device dimensions and designs, and facilitates the integration of multifunctionality onto the sensing platform. Rigid silicon substrates are not a prerequisite and NWFETs on flexible polymeric substrates were also recently demonstrated, with the added advantages of cost effectiveness and flexibility (Timko et al. 2009).

Alternatively, the device architecture can be modified by introducing the microfluidic channel and biomolecular interaction at the back gate of the transistor (Fig. 6b). In this configuration, the back gate of the LGFET is deposited with a thin gold layer and modified with probe molecules which interact specifically with the target analytes. The biomolecular interaction, in this case, alters the electronic properties of the device through the electrostatic gating mechanism, similar to all other architectures (Maehashi et al. 2004). Better biomolecular attachment control in this configuration can be expected from the well established gold-biomolecule chemistry. However, the use of planar substrate instead of the nanostructured material as the sensing element might limit the achievable sensitivity of the platform.

Figure 6c shows another approach using a two-step lamination process for LGFET fabrication (Tey et al. 2009), in which the use of silicon substrate is no longer required. The detailed fabrication process of this laminated CNT–LGFET is exemplified in Fig. 7. Only two materials are required in this fabrication route: SWCNT and PDMS. A thin SWCNT random network, formed from suspension through vacuum filtration method (Zhou et al. 2006), is transfer-printed from an alumina filter onto a blank PDMS substrate to form the semiconducting layer, while another thick, metallic-like SWNT random network prepared from the same methodology is transfer-printed onto another PDMS substrate (with an integrated microfluidic channel) as the electrode material. The stamping of CNT on the PDMS with the defined microchannel results in the auto-separation and formation of source–drain pads on each side of the microchannel. Lamination of the two PDMS substrates face-to-face encloses the microfluidic channel and completes the fabrication process. The integrated microchannel in this fabrication route plays an active role in forming the source–drain pads and defines the channel length of the transistor in addition to flow control. The main advantage of this process is that it eliminates photolithography, integrates the microfluidic channel and transistor fabrication into one step and simplifies the source–drain deposition and alignment through transfer printing and auto-alignment capability. Furthermore, the employment of random network in lieu of single nanotubes improves the batch-to-batch repeatability of the measurement, although potentially at a slight expense of the sensitivity due to the tube-to-tube contact resistance. This methodology is extendable to other semiconductor materials such as graphene and oxide nanowires. The PDMS substrate may readily be replaced with other polymers such as moldable plastics as substrate materials and thus this microfluidic-integrated LGFET based on facile fabrication methods and solution processed semiconducting materials, holds great potential for low cost, disposable lab-on-a-chip devices for field applications.

It is thus evident that a wide variety of approaches have been pursued to establish a robust fabrication platform for CNTs/NWs-based transistors. Fabrication processes which yield stable microfluidic-integrated transistor devices and are scalable toward mass-production would be critical for the realization of CNTs/NWs transistor-based sensors for label-free detection of bioanalytes in aqueous media.

3.4 Device factors affecting the biosensing performance in microfluidic-integrated transistors

The CNTs and NWs have proven themselves as a versatile interface for biomolecules attachment and detection, with potential applications in fields as diverse as healthcare (Wang et al. 2007; Zhang et al. 2007), defense (Patolsky

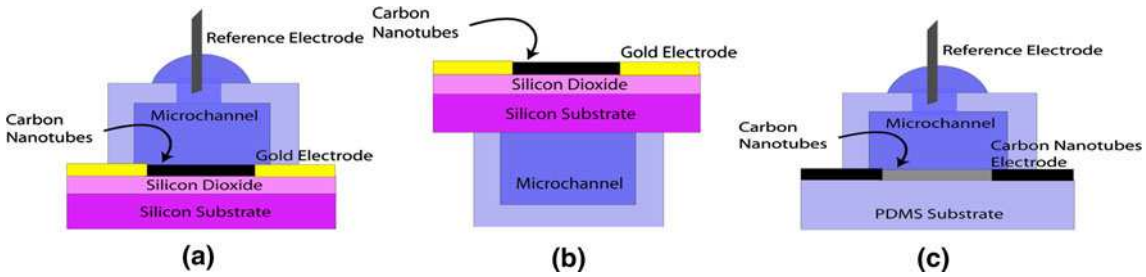

Fig. 6 Different device architectures with integrated microchannel. **a** The most conventional configuration where the microchannel is placed on top of the device. **b** The microchannel is placed around the back gate. **c** The source–drain electrodes and microchannel are integrated into one process step and stamp on top of the semiconducting channel region

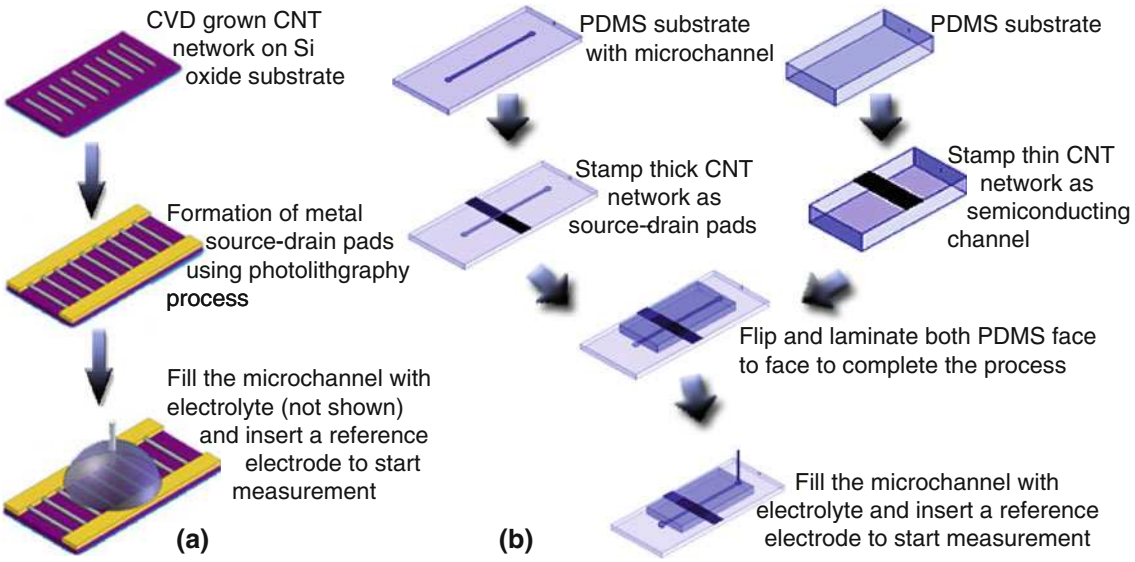

Fig. 7 **a** Fabrication of a conventional Si based LGFET. CNTs are first grown on silicon oxide substrate using CVD process, followed by electrode deposition and PDMS sealing to introduce microfluidic channel on top of the sensing region. The fabrication steps involve high temperature growth and high cost photolithography and metal deposition process. In contrast, fabrication of laminated, all CNTs, PDMS-based LGFET in **b** simplifies the fabrication process and is amenable to production of low-cost biosensors

et al. 2006c; Lee et al. 2009), and environmental monitoring (Hussain et al. 2009). Although their high surface-to-volume ratio constitutes their extreme sensitivity, it also implies that the conductance can be influenced easily by factors unrelated to the biomolecular interactions of interest.

As highlighted below using examples of NW- and CNT-based sensors, a number of factors need to be accounted for in analyzing the sensing performance of these biosensors. Indium Oxide (In_2O_3) nanowires (Curreli et al. 2008) used in detection of prostate specific antigen (PSA), in 1× phosphate buffer saline (PBS) solution displayed detection limits of 7 pM, whereas SWCNTs (Maehashi et al. 2006) showed limits of 250 pM for the detection of Immunoglobulin E (IgE) with aptamer probe molecules in 10 mM PBS. The different ranges in detection limits highlight the need for taking into account several factors that influence biosensor performance.

In general, the biosensing performance of a LGFET is affected by both the external environment and the intrinsic properties of the biomolecule and CNT/NWs such as ionic strength of the buffer solution, microchannel design, size of the biomolecules, metal/semiconductor contact area, and type of gate electrode employed, among others. A proper selection of experimental parameters and platform design are therefore crucial to ensure the validity of the detection signal, preventing false positive sensing, and optimizing the sensitivity of detection. The microfluidic device related considerations are discussed in this section whereas the biomolecular interactions related factors are discussed in subsequent sections.

3.4.1 *Electrolyte*

The ionic strength of the background solution has a significant contribution to the sensing signal. The presence of counter-ions in the solution leads to complete or partial neutralization of the charge and/or dipole moment that are present on the surface of the biomolecule (Curreli et al. 2008; Poghossian et al. 2005; So et al. 2005). As a result of this charge screening, the electrostatic potential originating from the biomolecule surface decays in an exponential fashion, and its penetration depth into the bulk solution is governed by the Debye length (λ_D) (Israelachvili 1991; Poghossian et al. 2005):

$$\lambda_D = \sqrt{\frac{\varepsilon_r \varepsilon_0 kT}{2z^2 e^2 I}} \tag{2}$$

As mentioned in Eq. 2, the λ_D is influenced by several factors: (1) the relative permittivity of the dielectric (ε_r), which depends on the solvent ($\varepsilon_r = 78$ for water); (2) temperature ($T = 300$ K in standard condition), (3) the valency of the counter-ions (z), and (4) the ionic strength of the solution (I).

The importance of ionic strength is evident when SWCNT–LGFET exposed to Poly(L-Lysine) (PLL) at a fixed concentration (1 μM) in de-ionized water of differing ionic strengths. The ionic strengths were modulated by changing either the ion valency: K^+, Ca^{2+}, and Al^{3+} (10^{-4} M); or their concentration: KCl at 10^{-4}, 10^{-2}, and 1 M. At neutral pH typical of water, the PLL molecules assume positive charge due to their high isoelectric point (p$I = 9.8$), as depicted in Fig. 8a. Upon attachment, the

positively charged PLL induces a reduction in the hole carriers in the nanotubes, leading to a drop of the source–drain current (I_{DS}). Varying the ionic strength of the electrolyte solution by either augmenting the ion valency or concentration results in a reduction in the LGFET conductance (Fig. 8b, c) and the degradation of its sensitivity, similar to other reported results (Curreli et al. 2008; Maehashi et al. 2006; Li et al. 2005; Poghossian et al. 2005).

Similar observation may also be noted in NW-based sensors. Detection of several cancer biomarkers with SiNWs in diluted buffer media having $\lambda_D \sim 130$ nm reported a detection limit of $\sim$2 fM (Zheng et al. 2005). In contrast, PSA detection (Li et al. 2005) with In_2O_3 NWs in undiluted PBS buffer having $\lambda_D \sim 0.8$ nm could only achieve detection limit $\sim$8 pM. Even though the type of NWs employed in these two reports differs, the ionic strength of the background solution undoubtedly contributed to the detection limits (Zheng et al. 2005). It is hence important to select a buffer that yields an appropriate Debye length that augments the LGFET sensing response (Stern et al. 2007b).

Another factor that warrants consideration is the pH of the electrolyte which influences the overall charge of a given biomolecule. Adjusting the pH below the isoelectric point of a given biomolecule will lead to an overall net positive charge while the opposite holds for pH above the isoelectric point, hence affecting the resultant electrostatic gating influence on the CNT/NW networks. In addition, the change in net charge of the biomolecules will directly alter the binding constant to the complementary biomolecules, resulting in a loss of the binding efficiency.

3.4.2 *Device architectures*

The influence of device configuration has been studied through modeling and simulation (Kim and Zheng 2008), taking into account the fundamental kinetic reaction between the biomolecules, convection in the fluid medium, and the diffusion mass-transport of target bioanalytes to the corresponding probe molecules. Diffusion is seen as the limiting factor to attain high sensitivity within a reasonable experimentation time. In this perspective, three possible actions are suggested to tackle this diffusion limit: (1) device substrate passivation, (2) microfluidic channel modification, and (3) suspending the CNTs/NWs in the middle of the microchannel (Fig. 9). All these approaches aim to raise the local concentration of the bio-analytes in the vicinity of the CNTs/NWs, and hence shorten the diffusion time.

In addition, our calculations also reveal that diffusion indeed plays an important role in determining the logical incubation time that can be used in the experimentation. In particular, the minimum expected diffusion time was

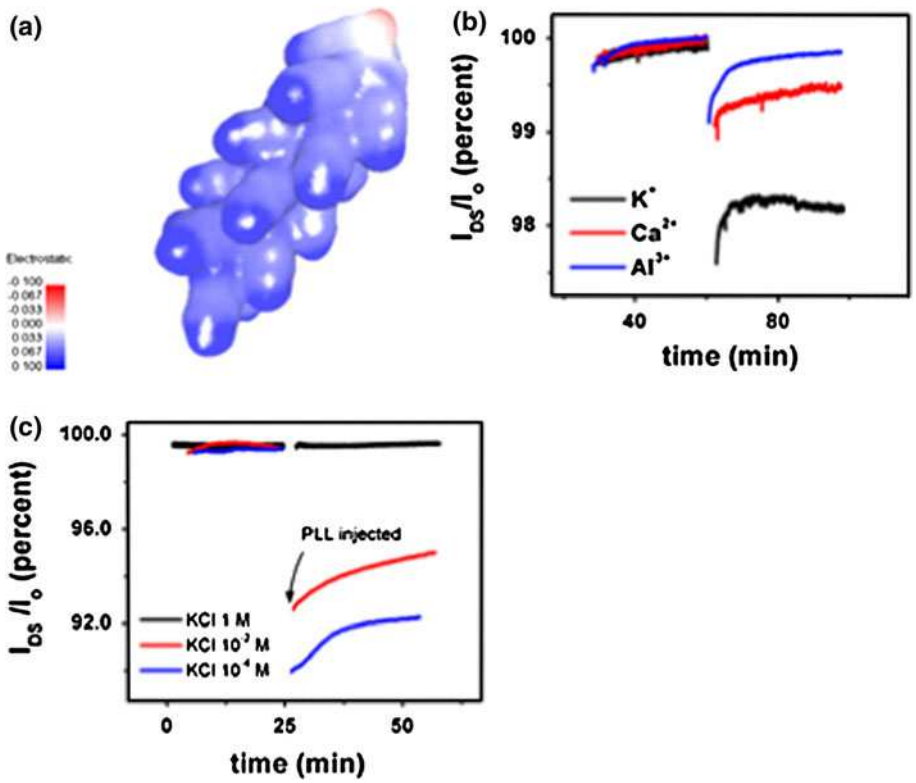

Fig. 8 **a** Electrostatic potential distribution on the surface of a PLL molecule. At neutral pH, the molecule assumes positive charge due to its high isoelectric point (p*I* 9.8). The signal level in SWCNT LGFET upon exposure toward the PLL at different ionic strengths, modulated by either **b** altering the valence of the ions: K^+, Ca^{2+}, and Al^{3+} (10^{-4} M), or **c** concentration of the ions: KCl 10^{-4}, 10^{-2}, and 1 M. The signal level in the LGFET dwindles as the ionic strength is increased

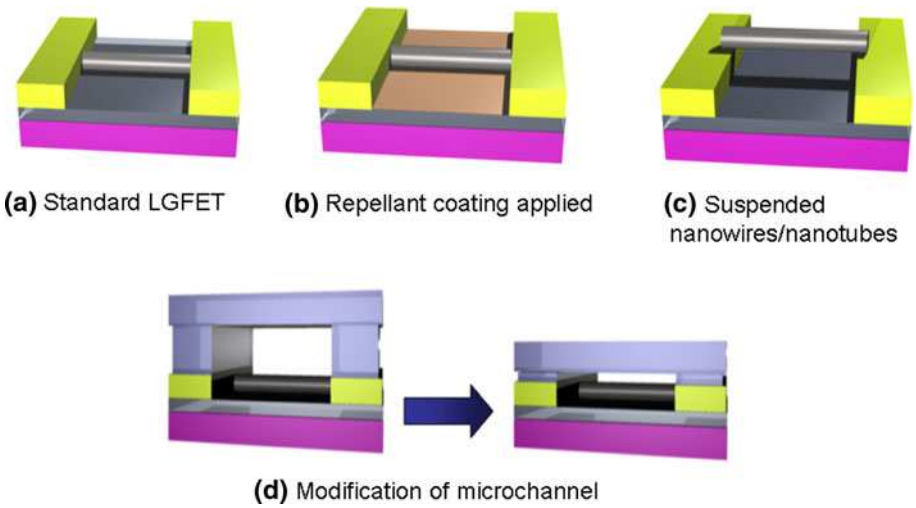

Fig. 9 Suggested methods to improve the sensitivity of a nanotube/nanowires LGFET based on calculation as performed in Kim and Zheng (2008). **a** A standard LGFET here is compared against modified devices, such as **b** passivation of device substrate with repellant coating, **c** suspended nanotube/nanowires, or **d** modification of microchannel; to improve the sensitivity

calculated by solving Fick's second law of diffusion to obtain the spatio-temporal distribution of the biomolecule concentrations in a microchannel (Fig. 10). Using typical diffusion constant for proteins (Brune and Kim 1993), and in accordance with other reports (Kim and Zheng 2008), it is found that a minimum incubation time of 10 min is expected for a typical micro-channel depth of 20 μm. The incubation time may be reduced if the microchannel height is decreased and/or the local bioanalyte concentration surrounding the CNTs/NWs is increased.

3.4.3 *Operating bias frequency and range*

The ability of LGFETs to operate in aqueous liquid media is an advantage because it allows the device to monitor the biomolecular interaction in their most native environment.

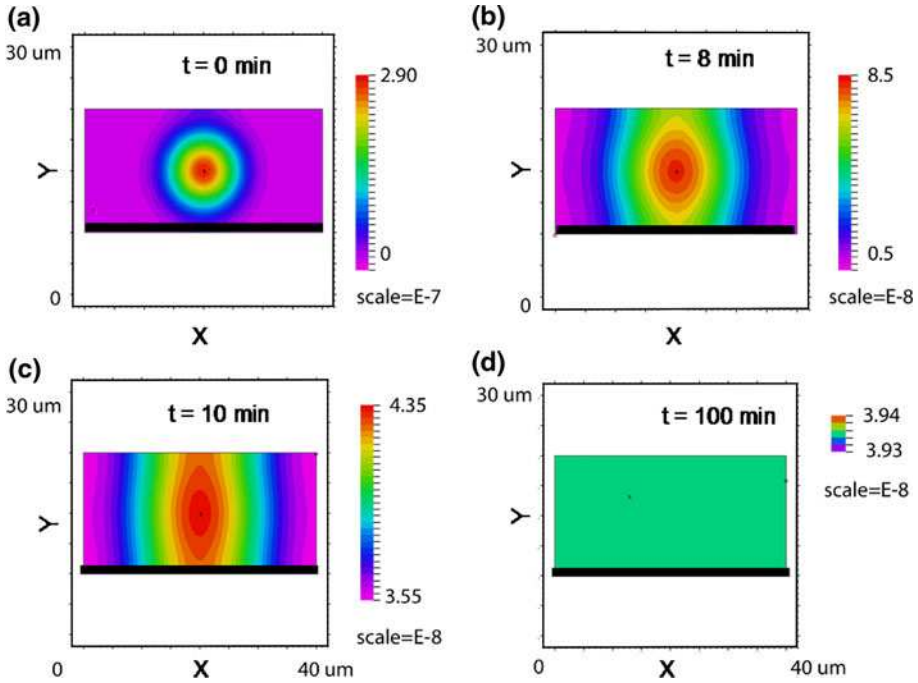

Fig. 10 Spatio-temporal distribution of protein concentration in a microchannel at time 0–100 min as obtained from solving Fick's second law of diffusion shown in **a**–**d**, consecutively. From these results, it can be estimated that the minimum amount of time to incubate the biomolecule is ~10 min, which corresponds to the time at which the biomolecules cover the entire base of the microchannel. The *X* and *Y* represent the cross-section of a microchannel (width 40 μm, height 10 μm). The simulation assumes that the biomolecule spread from the center of the microchannel at $t = 0$ min. The *solid rectangle* at the bottom of each figures represent the position of the CNT/NW film. The *color bar* in each figure corresponds to the concentration range (in Molar) in the microchannel at specific time and space. Note that as time passes, the spread between the maxima and minima concentration diminishes, indicative of homogenization, as expected from the law of diffusion

Nonetheless, the requirement to apply V_G bias to the liquid sample brings a disadvantage in that the applied operating window is limited within ±1 V to avoid electrolysis of water, which can impart erroneous conductance measurements. In this context, a pulsating gate bias (Wijaya et al. 2010a) can be applied to kinetically avoid the electrolysis reaction, allowing the LGFET to be operated at V_G bias greater than ±1 V. The principle of pulsed-gating to overcome the electrolysis limit is by taking advantage of the fact that electrolysis needs a certain amount of time to complete, which is typically in the range of 1 ms (Brady et al. 2000; Wang 2002). Hence, by applying a pulsating V_G with frequency greater than 1 kHz, the chemical reaction can be avoided altogether, while allowing the operating window to be extended to greater than ±1 V.

The pulsed-gating methodology can be used to perform both kinetic and I_{DS}–V_G measurements, with an appropriate modification of the pulse time-profile for the corresponding measurements, as revealed in Fig. 11a, b, respectively. The kinetic measurement which requires a constant level of V_G can be attained with pulsed-gating by applying a string of pulses with constant magnitude (Fig. 11a), while $I_{DS}V_G$ measurement which necessitates sweeping application of V_G bias within specific window can be performed with pulsed-gating by sending a string of pulses with modulating magnitude whose envelope is that of triangular waveform (Fig. 11b). The success of pulsed-gating to avoid the electrolysis reaction in this case can be observed in Fig. 11c, which displays an I_{DS}–V_G data for DC sweep and pulsed-gating across $-2 \leq V_G \leq 0$ window. The downtrend in I_{DS}–V_G for DC sweep at $|V_G| > 1$ volt marks the onset of the electrolysis reaction, which is in contrast to the I_{DS}–V_G of pulsed-gating showing a persistent I_{DS} increase, even at high V_G range indicating absence of the electrolysis reaction taking place in the solution. The access to larger operating window and higher I_{DS} level can be exploited as a route to improve the sensitivity of the CNT/NW–LGFET biosensor by taking advantage of the various possible sensing mechanisms that are operational at different V_G ranges.

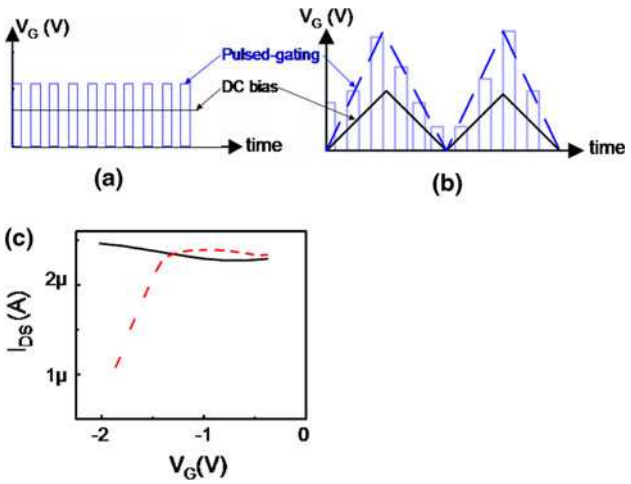

Fig. 11 V_G bias time-profile for DC and pulsed-gating in **a** kinetic and **b** I_{DS}–V_G measurement. Each pulse in the pulsed-gating lasts in a fraction of 1 ms, and hence avoids the electrolysis reaction kinetically, while allowing high V_G values to be applied to the LGFET. Evidence of kinetic avoidance of the electrolysis reaction is shown in **c** which compares the I_{DS}–V_G obtained from DC bias (*dashed red*) and pulsed-gating (*black*). The downturn in I_{DS}–V_G at $|V_G| > 1$ volt in **c** marks the onset of electrolysis reaction, while absent of such reaction is evidenced from persistent uptrend in the I_{DS}–V_G even at $|V_G| > 1$ volt window when pulsed-gating is applied. Image adapted from Wijaya et al. (2010a). Reproduced by permission from The Royal Society of Chemistry

3.4.4 Electrode

The CNT/NW transistor biosensors respond to the modulation of electrostatic potential in its immediate surrounding. The primary sources of modulation come from the biomolecular binding events and the application of gate bias (V_G). However, an improper choice of bare metal wire as the gate bias source may contribute to a false electrostatic potential modulation signal due to the interface potential of the exposed metallic wire to the electrolyte environment (Chen et al. 2001, 2004; Rosenblatt et al. 2002). It was shown in a later study that the surface potential of a platinum wire as gate electrode changes considerably upon exposure to proteins, through an open circuit potential measurement relative to a reference electrode (Minot et al. 2007).

Besides the gate electrode, the source–drain electrode is also another concern as mentioned in Sect. 2.3 in discerning the true underlying sensing mechanism. With an exposed source–drain contacts to the electrolyte, the biomolecular event can influence the work function of the metallic materials of the electrodes, altering the height of the Schottky barrier at the metal/semiconductor junction, leading to a modulation in the I_{DS} detectable through electrical measurement (Gui et al. 2006; Dong et al. 2008; Byon and Choi 2006). This Schottky barrier effect exists in both CNT- and NW-transistor unless top–down approach is adopted for the NWFET fabrication or additional annealing treatment is carried out to ensure an ohmic contact at the junction of two interfaces (Cui et al. 2003).

Isolating the source–drain electrodes from the surrounding aqueous medium is the best logical way to prevent the contribution from Schottky modulation that complicates the signal analysis. It is thus important to use a standard reference electrode as gate electrode to prevent the direct contact of metal wire with the electrolyte solution, and through contact passivation to confine the biomolecular event solely to the channel region.

4 Biomolecule—nanotube/nanowire interactions and its influence on biosensing

The previous sections have emphasized device aspects of the biosensor. In this section, the advancement of LGFET-based biosensing will be addressed, with examples of different biomolecules and their contrasting sensing response. In addition, molecular factors such as the characteristics of biomolecules and the CNT or NW which plays a major role in determining the performance and sensitivity of the LGFET will be detailed in this section.

4.1 Molecular factors affecting the biosensing performance in microfluidic-integrated transistors

4.1.1 Biomolecules: size, structure and conformation

Most biomolecules are complex, large in size (from 1 nm to few μm), comprise multiple molecular units, which may confer a hydrophilic and/or hydrophobic character. The hydrophilicity of biomolecules arises because they either have a net charge, or a dipole moment, and the charge is influenced by the pH of the electrolyte as mentioned in Sect. 3.4.1, which affects the interaction with nanotubes. Besides the charge effect, understanding the impact of Debye length has led to the awareness of the size effect of biomolecules, particularly the receptor molecules, on the detection limit of a sensing platform.

Typically, the size of antibodies range between 10 and 15 nm (Rudikoff and Potter 1976; Teillaud et al. 1983). In the case of immunosensing using the direct detection approach (Kojima et al. 2005), it is very likely that the antibody receptor–antigen recognition binding would occur outside the electrical double layer of a buffer solution with a millimolar salt concentration. In this respect, receptors of smaller size but equally high recognition and selectivity ability are employed to improve the sensitivity of detection.

Aptamers have been used to replace the antibody receptors for specific antigen detection. Aptamers are artificial oligonucleotides (DNA or RNA) with size of 1–2 nm that can be generated and engineered to recognize a wide variety of entities such as small organic molecules, amino acids, drugs, proteins, and cells with high specificity (So et al. 2005; Maehashi et al. 2006) (Fig. 12a, b). Given its much smaller size compared to antibodies, the aptamer–protein interaction can be brought closer to the CNT/NW surface within the Debye length (~3 nm for 10 mM ionic concentration) for effective signal detection on the receptor–ligand binding event. Example of thrombin (36 kDa) detection using this configuration, with SWCNTs as the transducer element, attained detection limit of approximately 10 nM (So et al. 2005). The sensitivity improvement was related to the relative size of thrombin as compared to that of the aptamer; which introduces considerable electrostatic potential disturbance in the immediate vicinity of the nanotubes and resulting in an improvement in sensitivity. Another similar approach involves the use of cleaved immunoglobulin fragments for immunoglobulin G detection (Fig. 12c), with reported detection limit of 1 pg/ml (Kim et al. 2008).

In another study, an indirect detection strategy was adopted (Tey et al. 2010; Wijaya et al. 2010b). In this approach, the target analytes are first conjugated to protein molecules, followed by immobilization of the hapten–protein structures to the CNT, and subsequently the specific antibody detection (Fig. 13). As the size of hapten–protein conjugate is smaller than the antibody, the strategy allows the recognition process to be held closer to the semiconducting channel. The key concept of the indirect, competitive assay used in the study lies in pre-mixing the antibody solution of fixed concentration with a varying concentration of target analytes prior to the solution

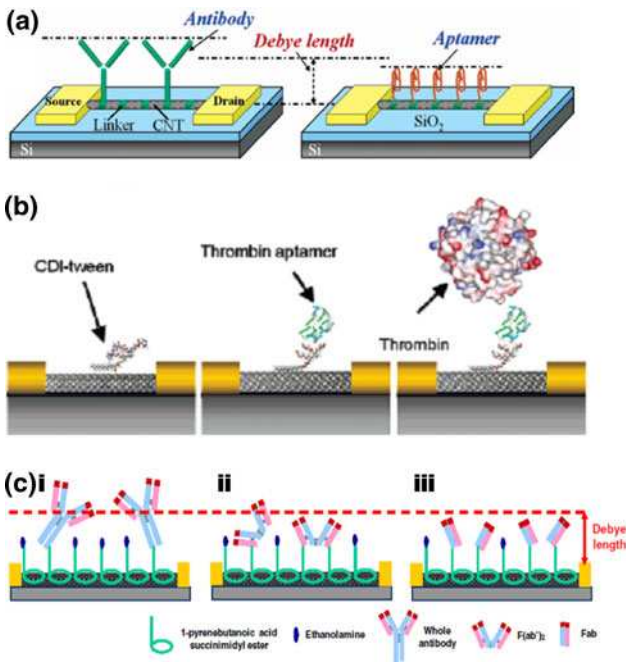

Fig. 12 **a** Schematic illustration of an antibody-modified and aptamer-modified CNT–LGFET biosensor. Reprinted with permission from Maehashi et al. (2006). Copyright (2006) American Chemical Society. **b** Example of thrombin detection using aptamer receptor. Reprinted with permission from So et al. (2005). Copyright (2005) American Chemical Society. **c** Schematic diagram of CNT–FETs modified with three types of receptors on CNT surface: (i) immobilization of whole antibody; (ii) immobilization of cleaved fragment consists of two Fabs; and (iii) immobilization of cleaved fragment with single Fab. The use of active Fab fragment brings the subsequent immune-binding reaction to within the Debye length distance from the CNT surface, leading to enhanced detection. Image adapted from Kim et al. (2008). Reprinted with permission from Elsevier

injection onto the sensing platform, which leads to a mixture of antibody–antigen conjugates with excess free antibody moieties (Fig. 13ii). Upon injection of the solution mixture, the free antibodies compete for binding with the hapten–protein conjugate receptors, resulting in a change in electrical signal (Fig. 13iii). By determining the concentration of the free antibodies, one could back-track the initial concentration of the target analytes. The methodology was used to demonstrate the detection of small target analyte, in which a direct detection approach is insufficient to generate significant disturbance signal to be detected by the underlying CNT channel, an intrinsic weakness of CNT- or NW-based electrical detection.

Thus far, we have only discussed the detection of biomolecules which have a charge associated with them. The detection of uncharged target analyte was elegantly demonstrated on SiNW–FET via the participation of a reporter protein molecule (Chang et al. 2009). The charged reporter molecule (1,5-EDANS moiety) was chemically attached to the capture probe (Δ^5-3-ketosteroid isomerase, "Art_KSI"), followed by immobilization on the surface of the SiNW. In the presence of uncharged steroid target analyte (19-norandrostendione, "19-NA"), the negatively charged reporter is expelled from the binding site and as it presents itself to the NW surface, an electrical response is generated (Fig. 14a), with sensitivities down to the femtomolar levels.

4.1.2 Types of CNTs and NWs

Wide-ranging understanding and control of nanowire properties has facilitated extensive research in improving the sensitivity of NW biosensors. The sensitivity of a NW-based FET biosensor is affected by the size (Elfström et al. 2007), surface chemistry (Bunimovich et al. 2006), and doping density (Hahm and Lieber 2004) of the nanowire. The smaller the diameter of the nanowire, the larger the surface-to-volume ratio and thus the surface charges on the sidewall of the nanowires will become increasingly important to influence the charge density in the channel. Simulation results show that the nanowire with diameters beyond 150 nm are virtually insensitive to external environments (Elfström et al. 2007). In addition to the diameter effect, different surface chemistries will also affect the biosensor performance of SiNWs. With the presence of native oxide on the surface of NWs, the sensitivity was found to degrade significantly. The poor performance was attributed to the presence of interfacial electronic states on the surface, and the screening effect caused by the insulating oxide layer to biomolecular interaction event. By removing the native oxide and directly attaching linkers to the H-terminated SiNW surface, improved sensitivity was achieved (Bunimovich et al. 2006).

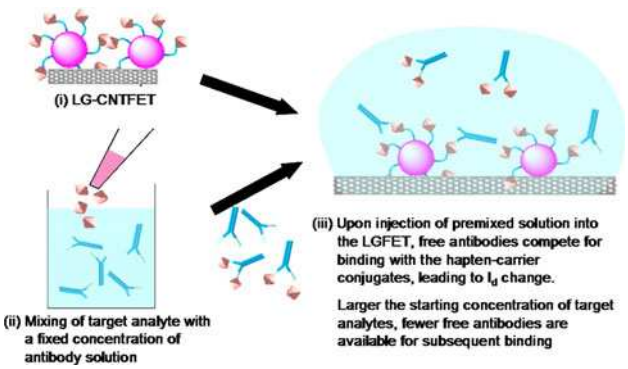

Fig. 13 Schematic showing the competitive assay approach for indirect detection of target analyte

Similar to the effect of ionic strength of an electrolyte that screens the charge/dipole moment of target analytes (Sect. 3.4.1), high doping concentrations result in reducing the screening length in SiNWs. Therefore, any interference signal resulting from the binding of biomolecules on the sidewalls can only gate the surface layer rather than the entire volume of NWs (Gao et al. 2009). This influential parameter is absent in SWCNTs. Although both the CNTs and NWs belong to quasi one-dimensional nanostructured materials, their atomic structures are distinctly different. The NWs typically assume a rigid, rod-like solid cylinder geometry; whereas the SWCNTs can be visualized as the roll-up of single layer graphene sheet into a hollow, tubular structure. Therefore, all its carbon atoms are residing on the surface, directly sensing the potential disturbance signal that originates from the immediate surrounding. From the molecular structure perspective, the SWCNTs should be more sensitive than the NWs for biosensing applications. Nevertheless, the drawback of the former, such as the uncontrollable electrical properties during growth and the limited functionalization strategies, have rendered the realization of CNT-related applications a yet-to-achieve target.

The sensitivity of a CNT–LGFET-based biosensors is affected by the tube diameter and chirality, which determines its semiconducting properties. Comparison of sensing performance between metallic and semiconducting SWCNTs has led to the conclusion that metallic SWCNTs are insensitive to molecule detection; while the sensitivity of semiconducting SWCNTs sensitivity is largely dependent on the slope of $I_D V_G$, i.e. the transconductance value: larger detection signal was observed with greater transconductance (Boussaad et al. 2003). Recent studies on both the CNT and NW–LGFETs revealed separately that a real-time biosensing that performed at the subthreshold regime displays the highest sensitivity by attaining the lowest signal-to-noise ratio (Heller et al. 2009) and highest percentage conductance response (Gao et al. 2010). In

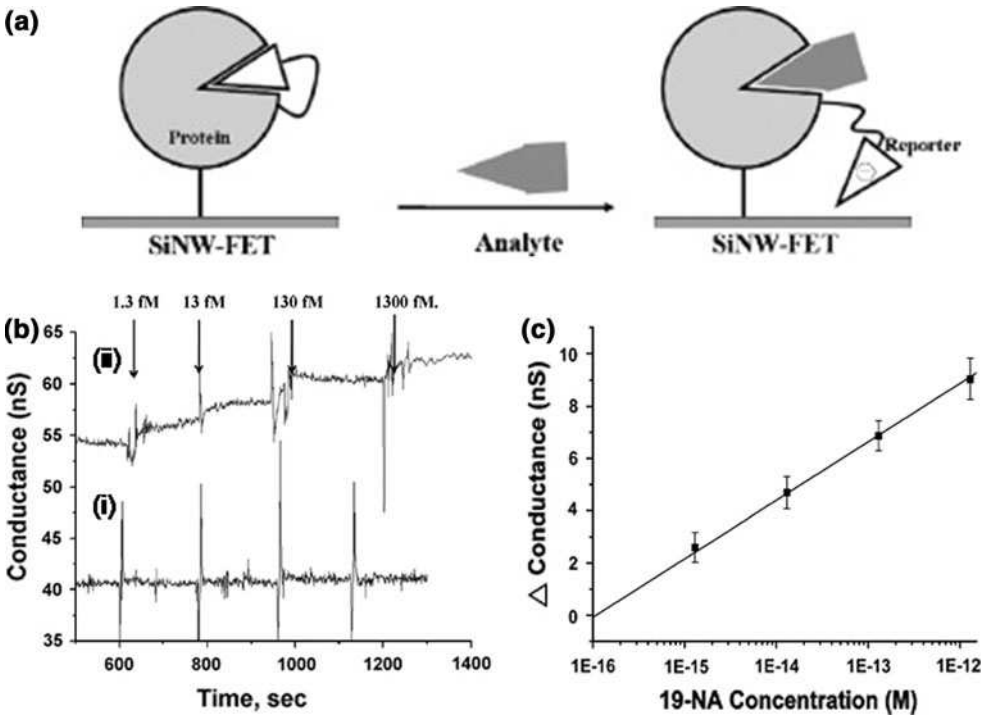

Fig. 14 **a** Illustration showing the design of a SiNW–FET for the detection of an uncharged analyte. **b** Comparison of the conductance response upon addition of 19-NA to NWFET labeled with (*i*) Art_KSI and (*ii*) Art_KSI/mA51. **c** The linear correlation of the change of conductance with respect to the concentration of 19-NA. Images adapted from Chang et al. (2009). Reprinted with permission from Elsevier

addition, the surface functionalization strategies would also influence the attachment of receptor biomolecules onto the CNT and NW sidewall through either covalent or non-covalent approaches which will be elaborated in further detail in the following sections.

4.1.3 Binding specificity

A common source of false signal contribution usually comes from non-specific binding of the non-target analytes to the CNT or NW channel. The undesired binding of non-target analytes can be prevented by imparting selectivity and specificity to the transistor sensing platform. These functionalities can be attained by functionalizing the CNTs/NWs with biomolecules. In this regard, the ability of biomolecules to specifically recognize their partner imparts specificity to the nanostructures. Hence, surface functionalization becomes a critical integral aspect in the development of CNT/NW–FETs.

For CNTFET, surface functionalization of CNTs with various biomolecules can be done using both non-covalent and covalent approaches. The former case has been shown in most direct detection studies, where the biomolecules absorb directly onto CNT through physisorption process, such as van der Waals force, hydrophobic interaction, or π–π stacking. However, one major drawback for physisorption is that receptor molecules are usually unstable and get dislodged during subsequent rinsing steps, causing signal inconsistency. A bifunctional linker molecule is therefore preferred to bridge between the receptor molecules and CNTs. The linker molecule usually has a hydrophobic end which allows a strong interaction with CNTs, and a hydrophilic end to allow flexibility for covalent functionalization with receptor molecules. One of the most commonly used linker molecule is 1-pyrene-butanoic acid succinimidyl ester, which has proven to be highly stable against desorption (Chen et al. 2001) (Fig. 15a). The pyrene group absorbs irreversibly onto the hydrophobic sidewall of CNTs through π–π interaction, and the active ester group enables formation of amide bond through nucleophilic substitution of *N*-hydroxysuccinimide with an amine group on the protein. Tween-20 is another popular option as linker and blocking agent with similar functionality and reaction chemistry, as shown in Fig. 15b (Chen et al. 2003). In addition to small molecules, sidewall functionalization of CNTs has also been demonstrated with polymers (Dong et al. 2008; Star et al. 2003; Martinez et al. 2009). Apart from the ability to prevent non-specific absorption, the polymeric shell can be further modified to covalently couple with receptor molecules for subsequent target specific recognition (Star et al. 2003; Martinez et al. 2009) (Fig. 15c).

Another functionalization approach in CNT is through direct covalent bonding with receptor molecules. This is achieved by introducing functional groups along the CNT sidewalls and is usually carried out during the post-synthesis step. One example is the generation of carboxylic side groups on the sidewalls of acid-treated CNTs. These carboxylated CNTs can be bound to biomolecules through diimide-activated amidation process (Jiang et al. 2004). 2-

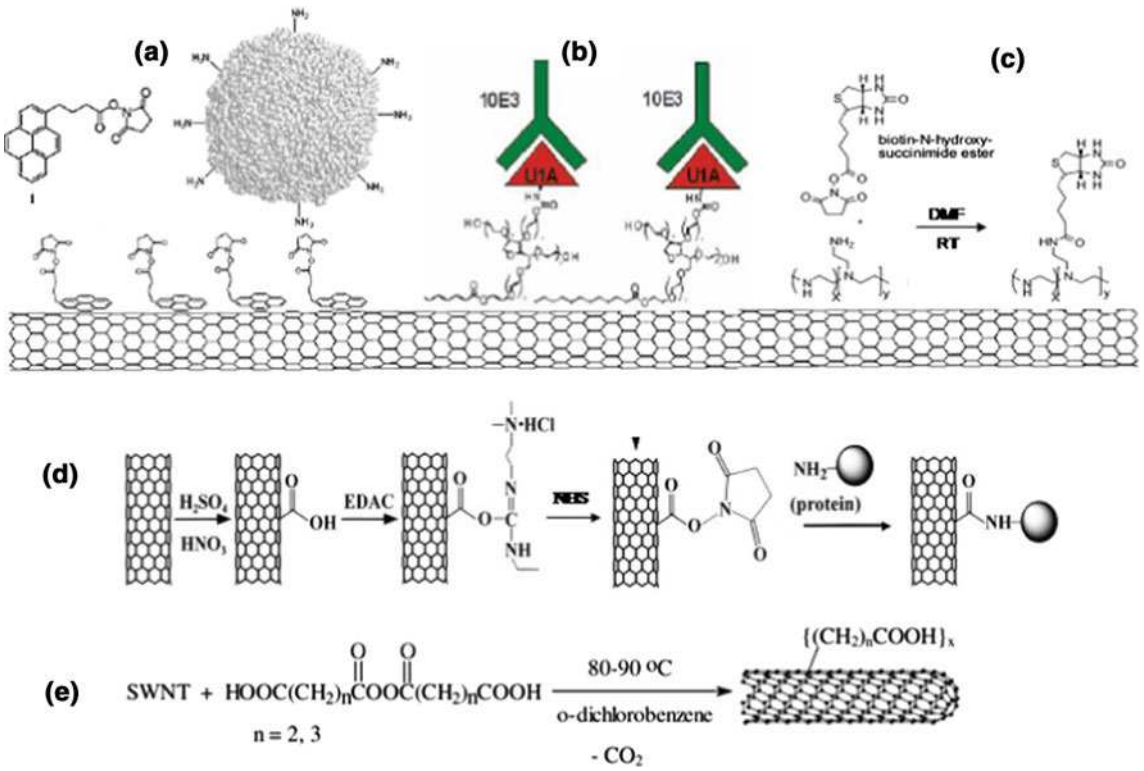

Fig. 15 Functionalization of CNTs through non-covalent **a**–**c** and covalent approaches **d**–**e**. **a** 1-Pyrenebutanoic acid, succinimidyl ester irreversibly adsorbs via π-stacking of pyrene base onto the sidewall of SWNT. Adapted with permission from Chen et al. (2001). Copyright (2001) American Chemical Society. Similarly for **b** tween-20 with its aliphatic carbon backbone absorbs onto the sidewall. The dangling end groups extending out of the tube can be further modified for subsequent biomolecules binding (Chen et al. 2003). Copyright (2003) National Academy of Sciences, U.S.A. **c** Use of polyethyleneimide (PEI) as blocking layer and linker for subsequent receptor attachment. Adapted with permission from Star et al. (2003). Copyright (2003) American Chemical Society. **d** Carboxylation of CNT through acid reflux for direct linking of receptor molecules to the CNT sidewall via two-step process of diimide-activated amidation (Jiang et al. 2004). Reproduced by permission of The Royal Society of Chemistry. **e** Reaction of SWNT with acyl peroxide in *o*-dichlorobenzene at 80–90°C to generate 2-carboxyethyl or 3-carboxypropyl radical for sidewall acid functionalization. Adapted with permission from Peng et al. (2003). Copyright (2003) American Chemical Society

carboxyethyl or 3-carboxypropyl side groups can also be created on the CNT sidewalls by reacting CNTs with succinic or glutaric acid acyl peroxides in *o*-dichlorobenzene at elevated temperature (80–90°C). The side groups can be further converted to acid chlorides by the derivatization with $SOCl_2$ (Peng et al. 2003) (Fig. 15d, e). In a recent study on the interaction of BSA with pristine and carboxylated SWNTs, carboxylated SWNT appeared to have stronger interaction with BSA, as evidenced from greater change in conductance signal and conformation of the structure (Wijaya et al. 2009).

In the case of NWFETs, surface functionalization scheme depends on the terminal groups present on the SiNW surface. For hydroxyl-terminated SiNW where there is a thin native oxide layer on the surface, surface modifications can be done using SAMs of silane derivatives: $R(CH_2)_nSiX_3$ (X = Cl, OCH_3, or OC_2H_5; R = surface group, e.g., CH_3, NH_2, SH, $CH=CH_2$, etc.) (Chauhan et al. 2008), with the surface groups that are accessible for subsequent immobilization of receptor molecules. Examples of the most widely used alkoxysilane derivative linkers are 3-(trimethoxysilyl)propyl aldehyde (Patolsky et al. 2004, 2006b; Zheng et al. 2005; Gao et al. 2007), 3-aminopropyltriethoxysilane (Kim et al. 2007a; Cui et al. 2001), and 3-mercaptopropyltrimethoxysilane (Curreli et al. 2008). For all these SAMs, the Si-methoxide or Si-ethoxide end groups of the linkers react to form a strong covalent bond with native silicon oxide layers (Fig. 16a), and the surface groups at the other end of the molecules have to be carefully selected such that they are compatible with subsequent functionalization with biomolecule receptors.

Although the native oxide coating on SiNW serves as an effective layer for functionalization with a bioaffinity moiety, this oxidized surface can lower or limit the sensor performance (Zhang et al. 2008b). In addition,

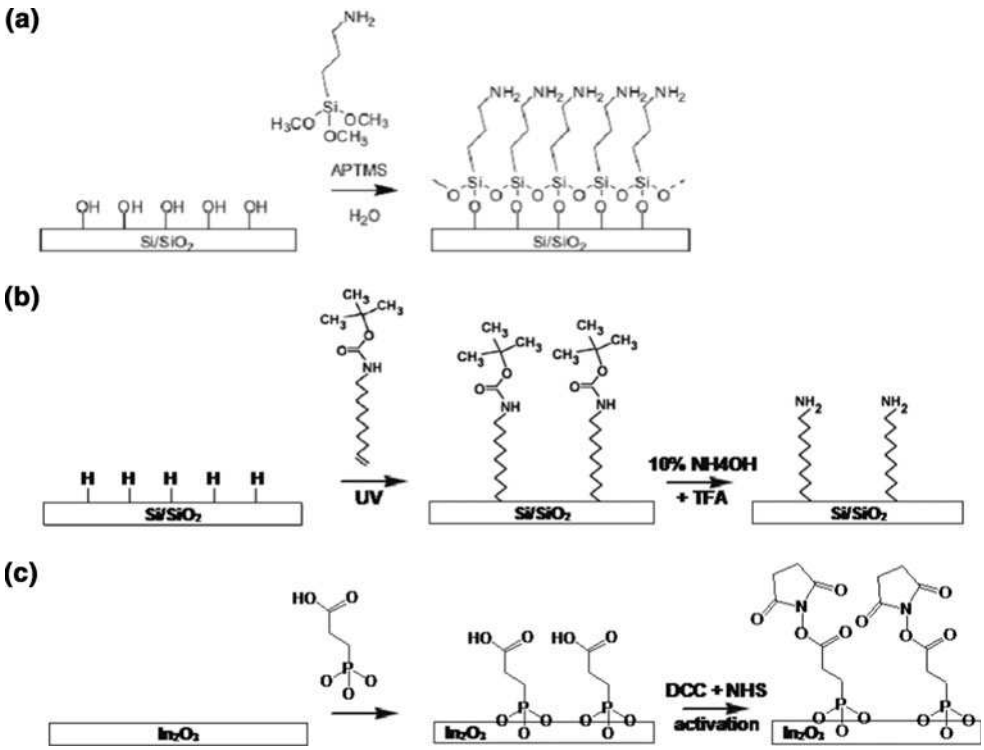

Fig. 16 Schemes for NWs functionalization. **a** Alkoxysilane treatment on SiO_2/SiNW to produce amine- (shown in the figure) or aldehyde- (not shown here) terminated surface (Chauhan et al. 2008). With kind permission from Springer Science+Business Media. **b** For H-terminated SiNW, photochemical hydrosilation reaction was employed to attach unsaturated C=C bond to the surface. **c** Phosphonate derivatives functionalization of metal oxide NW by deposition from aqueous solutions

inhomogeneity and variability in the relative number of Si–O–Si and Si–OH linkages can lead to reproducibility and homogeneity issues for bio species-modified surfaces (Strother et al. 2000). In this regard, chemical pathways for direct SAM functionalization on silicon surface opened up new possibilities for highly controlled biomolecules attachment with improved detection sensitivity. The native oxide coating can be etched away with hydrofluoric acid (HF), forming hydride-terminated silicon surface. The Si–H bond can undergo two-step chlorination/alkylation route to engender methyl-functionalized SiNWs. Improved sensor characteristic with less hysteresis has been reported with hydride and methyl-terminated SiNW (Haick et al. 2006). Alternatively, the hydride-terminal can also be converted to aminodecane-modified silicon surface via photochemical hydrosilation reaction (Zhang et al. 2008b; Streifer et al. 2005; Stern et al. 2007a; Strother et al. 2000; Bunimovich et al. 2006) (Fig. 16b). The resulting amino groups can be coupled directly to antibody or thiol modified DNA using a heterobifunctional crosslinker (Stern et al. 2007a; Streifer et al. 2005), or are converted to aldehyde groups using glutaraldehydes, followed by coupling to amine terminated biomoieties (Zhang et al. 2008b).

For oxide metal nanowires such as In_2O_3, Sn_2O, and ZnO, a simple and mild self-assembling process utilizing phosphonic acid derivatives was reported (Fig. 16c) (Li et al. 2005; Curreli et al. 2005). The oxide nanowire was submerged in 3-phosphonopropionic acid aqueous solution, followed by carboxyl terminal group conversion to carboxylate succinimidyl ester via incubation in *N*,*N*′dicyclohexylcarbodiimide (DCC) and *N*-hydroxysuccinimide (NHS).

With a better understanding on the device and the molecular factors affecting the sensing performance and sensitivity of the biosensing platform, the application examples on a variety of biomolecules using CNT and NW–LGFET will be discussed in the following sections.

4.2 Sensing with single to few tubes/wires-LGFET platform

Depending on the assembly technique and channel size, the CNT- or NW-based FET platform can be classified into two broad categories based on the number of tubes across the channel: (1) devices which comprise of one or few tubes bridging the source-drain electrodes directly without inter-tube interaction and (2) nanonet devices with high density of overlapping and interconnected tube networks. The following paragraphs will focus on the biosensing examples performed using one or few tubes-/wires-based LGFETs.

Following the reports for CNT as a gas sensor in dry-state measurements (Kong et al. 2000), one of the first few efforts on single tube-LGFET biosensing was performed for glucose detection (Besteman et al. 2003). In this study, redox enzyme glucose oxidase (GOx) was attached to the CNT using linker molecule. Addition of 100 nM glucose to

the active sensing channel coated with GOx leads to an increase in conductance which was attributed to the catalytic reaction, where glucose is converted to gluconolactone, causing conformational changes in GOx and modifying the charge state of the functional groups on the GOx surface. Measurement with similar device configurations were carried out subsequently on direct streptavidin (Bradley et al. 2004) and cytochrome *c* (Boussaad et al. 2003) detection.

Detection of DNA hybridization is also an important aspect, with several reports in both dry and wet states. Here, we highlight a modified liquid-gated measurement for ultrasensitive DNA detection (Fig. 6b) (Maehashi et al. 2004). Amino-modified peptide nucleic acid (PNA) oligonucletides bound to SAM/Au surface were used as capture probes. The use of PNA is thought to reduce the charge repulsion and enhance base-pairing of PNA/DNA due to its neutral polypeptide backbone, thus leading to improved hybridization efficiency. Furthermore, because of reduced charge repulsion, lower ionic strength media can be used without compromising the hybridization efficiency, thus resulting in an increased sensitivity of detection. Subsequent DNA hybridization was brought about by flowing single-stranded DNAs across the back gate. Reported sensitivity was as low as 6.8 fM in this configuration (Maehashi et al. 2004).

For NW–LGFETs, all the device architectures employed to-date are based on single wire devices. Advancement of NWFET in biosensing applications was exceedingly successful even though the first demonstration for sensing study appeared later than CNTFETs (Cui et al. 2001). Most of the device platforms are in miniaturized format with integrated microfluidic channels, which can be readily implemented in real field applications. Biomolecules tested includes proteins (Cui et al. 2001), ATP molecules (Wang et al. 2005), viruses (Patolsky et al. 2004), cancer markers (Zheng et al. 2005), live mammalian neurons (Patolsky et al. 2006a), DNA/RNA (Gao et al. 2007), protein–protein interaction (Lin et al. 2010), to name a few.

With the aid of the mature micro-electronic fabrication technology, large-scale integration of NW–LGFET in arrays format is achievable, and multiplexing capability was demonstrated with high specificity and selectivity (Patolsky et al. 2004; Zheng et al. 2005). In these devices, arrays of nanowire transistors were first incubated with different receptor molecules. Upon injection of solution mixture which consists of target analyte and other biospecies into the microchannel, only the specific nanowire decorated with the right receptor molecules resulted in conductance change and the magnitude of the signal was proportional to the concentration of the analyte (Fig. 17a, b). The kinetic response of the measurement indicates the following features: (1) the detection is selective and specific; (2) the receptor-target binding is a reversible process; and (3) no measurable non-specific binding.

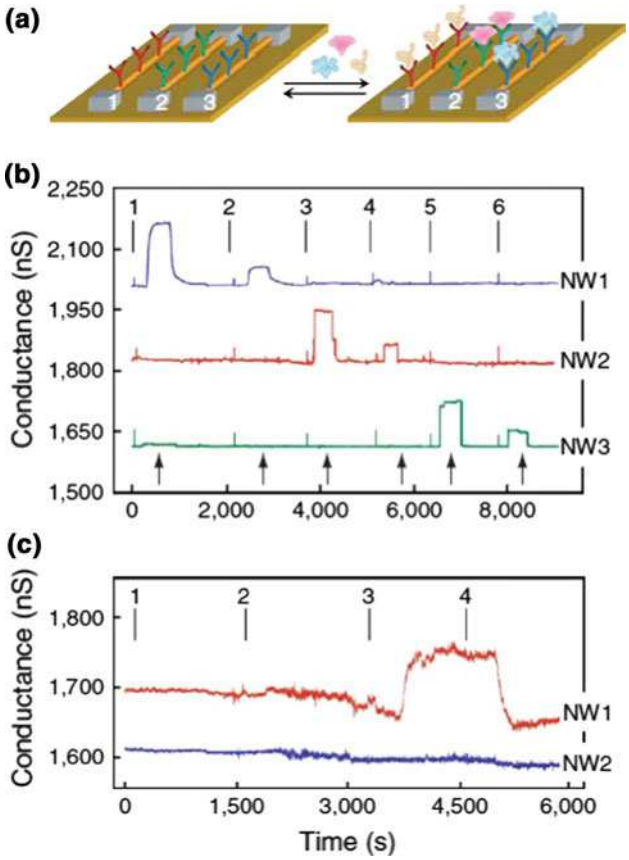

Fig. 17 **a** Schematic illustration of multiplexed detection of cancer marker proteins by three identical silicon nanowire devices with different antibodies. **b** Solutions containing PSA, CEA, and mucin-1 of two different concentrations were delivered to the nanowire array sequentially and specific detection was observed only on designated device with right receptor molecules. **c** PSA detection in undiluted human serum in which NW1 was functionalized with anti-PSA and NW2 was passivated with ethanolamine. Adapted by permission from Macmillan Publishers Ltd: Nature Biotechnology (Zheng et al. 2005), copyright (2005)

Using the multiplexing approach, detection limits obtained for PSA, carcinoembryonic antigen (CEA) and mucin-1 were 2, 0.55, and 0.49 fM, respectively, in phosphate buffer (PB) solution (Zheng et al. 2005). For PSA, further sensing was performed in desalted, undiluted serum sample. Detectable conductance change was observed at 27 fM PSA concentration, which is equivalent to about 100 billion times lower than the background serum proteins, demonstrating the potential for high sensitivity and selectivity detection of cancer markers in human serum (Fig. 17c).

PSA is a common choice of cancer markers used in both CNT and NW–FET sensing. By comparing the reported limit of detection (LOD) for both nanostructures, NW–LGFETs (LOD for PSA $\sim$ 2 fM) (Zheng et al. 2005)

appears to be more sensitive than CNT–LGFETs (LOD for PSA ~ 1.4 nM) (Li et al. 2005). However, it is inappropriate to arrive at any conclusions without and in-depth investigation of the parameters used in the experiment. The enormous difference lies on the fact that the measurement for NW–LGFET was conducted in a much diluted, 10 μM PB solution, which gave rise to Debye length of approximately 100 nm. This was in contrast to the 140 mM PBS solution in CNT–LGFET where Debye length was approximately 0.86 nm, in which charges from the analyte molecules were thought to be screened by the high ionic strength environment, drastically affecting the device sensitivity (refer to Sect. 3.4.1). The case study highlights the lack of standard testing protocols in CNT and NW–LGFET sensors.

In order not to compromise sensitivity, testing in low ionic strength buffer is appropriate. Nevertheless, this greatly reduces the clinical relevance of the CNT/NW–LGFET sensors where the target analytes are typically obtained from high ionic strength blood serum or serous fluids. This limitation was overcome by integrating the purification functionality into the biosensor, where the chip simultaneously captures multiple biomarkers from blood samples, washes, and releases them into purified buffer for detection. The two-stage approach enables direct electronic sensing of analytes from whole blood sample on a NW–LGFET sensing platform (Stern et al. 2010).

The interfacing of cells with NW and CNTFET is another successful demonstration for potential applications in medical monitoring and intervention for heart, brain, and other tissues. Examples of cultured neurons (Patolsky et al. 2006a), muscle cells (Pui et al. 2009), and embryonic chicken hearts (Timko et al. 2009) have been studied with high signal-to-noise ratios. The recent study integrates the multiplexing detection into the devices for the electrical recording of embryonic chicken cardiomyocytes (Cohen-Karni et al. 2009), using a flexible approach for the placement of cells on top of the NWs (Fig. 18).

Taking one step forward, a biosensor which mimics the biological means of communication for critical recognition, transport, and signal transduction would be the ultimate goal in the world of biosensing—a bionanoelectronic device. A hybrid platform combining the CNTs/NWs with protein membranes represents an important milestone toward the integration of biological components and manmade structures (Zhou et al. 2007; Misra et al. 2009). By incorporating the A pore channel into lipid bilayer membrane, the bionanoelectronic sensing platforms display positive ionic conductance response (Misra et al. 2009) (Fig. 19).

The NW–LGFETs discussed above rely mostly on bottom up fabrication approaches where the NWs are positioned onto desired channel regions through solution processing methods, as described previously in Sect. 3. To eliminate the randomness in NW positioning occurring in solution-based techniques, "top down" fabrication methods compatible with complementary metal oxide semiconductor (CMOS) FET technology was proposed (Stern et al. 2007a; Kim et al. 2007a). The "top–down" approach allows nanofabrication of nearly identical NWs with high reproducibility and throughput (Bunimovich et al. 2006), enabling system-scale integration with signal processing and information systems.

Using the top–down approach, real-time DNA detection using physiologically relevant 165 mM electrolyte solution was conducted on H-terminated SiNWs (Bunimovich et al. 2006). A noncovalent immobilization approach was adopted to circumvent the Debye screening effect from high ionic strength environment, where the receptor DNAs were absorbed electrostatically onto the amino-modified NWs and lying flat for the full length on the NWs. Upon hybridization, the full DNA duplex is also expected to lay

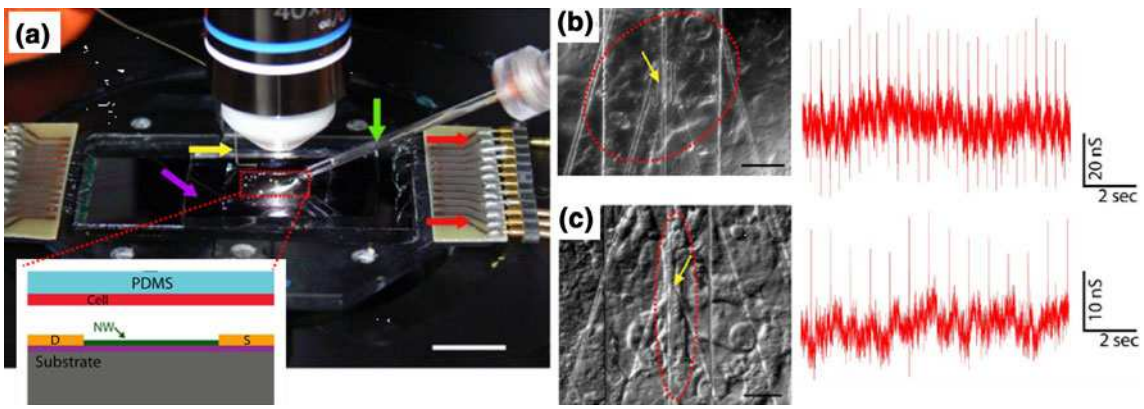

Fig. 18 **a** Measurement setup for cardiomyocyte signal detection. **b**, **c** Optical images showing the patch of beating cells and their respective conductance versus time signals on the right. Images adapted from Cohen-Karni et al. (2009)

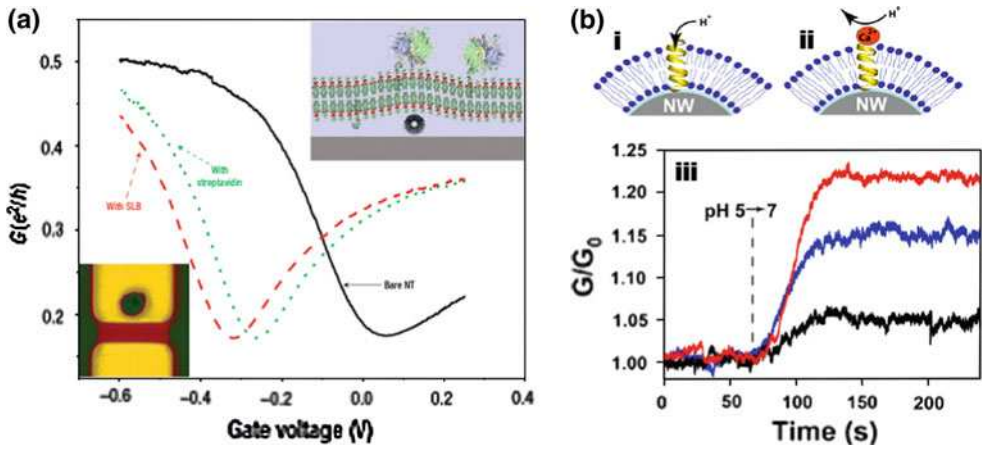

Fig. 19 **a** Conductance versus V_G measurement showing the conductance response of a CNTFET before (*solid black*) and after biotinylated supported lipid bilayer (*dashed red*) formation, and the response upon the binding of streptavidin to the membrane-embedded biotins (*dotted green*). **b** Device operation of liquid-gated NWFET incorporates gramicidin A pores. *i* and *ii* Schematic showing the proton transport in the bilayer incorporating a gramicidin A pore in the absence *i* and presence *ii* of Ca^{2+} ions. *iii* Kinetic measurement showing the device response upon the pH change from 5 to 7: *red trace* represents the uncoated NW device; *blue trace* represents the device coated with lipid bilayer incorporating gramicidin A; *black trace* denotes the device coated with lipid bilayer incorporating gramicidin A in the presence of Ca^{2+}. Image **a** adapted by permission from Macmillan Publishers Ltd: Nature Nanotechnology (Zhou et al. 2007), copyright (2007). Image **b** adapted from Misra et al. (2009)

flat on the NWs, thus bringing the influence of electrostatic change to within the Debye length distance. The lowest concentration used in the study was 10 pM. A lower DNA detection limit (25 fM) was reported later on using trimethyloxysilane aldehyde as the linker to immobilize amino-terminated PNA (Gao et al. 2007). This detection limit is in the same range reported in CNT–LGFETs. The fabrication process developed in the study enables etching of the NWs and bulk contacts as one piece and thus eliminates heterogeneous contact issues. In addition to DNA hybridization, better sensitivity of H-terminated SiNWs was also demonstrated for antigen detection. Specific label-free detection of immunoglobulin G and immunoglobulin A below 100 fM and streptavidin of 10 fM concentration were reported (Stern et al. 2007a).

4.3 Sensing with nanonet-LGFETs

As it can be appreciated from the previous sections, single/few CNT- and NW-based LGFETs have demonstrated its sensing capability toward a wide range of bio and chemical species. While the device performance of a NW–LGFETs have been shown to be consistent owing to well-controlled NWs properties from established fabrication techniques, single/few CNT–LGFETs often lead to irreproducible device characteristics due to a range of tube diameters and chiralities resulting from the growth process. The complexity and variation in device-to-device characteristics has rendered the implementation of multiplexing and system integration an impossible task. To address this intrinsic issue of CNT–LGFET, a random nanonet semiconducting CNT channel was offered as an alternative approach to average out the randomized effect in single/few CNT–LGFET.

The first specific biodetection using nanonet CNT–LGFET was demonstrated on streptavidin, human immunoglobulin (IgG), and monoclonal antibody for systemic lupus erythematosus and mixed connective tissue disease (Chen et al. 2003). Detection of these protein molecules was achieved by covalently functionalizing their counterparts, i.e., biotin, protein A, and U1A, respectively, to tween-20, which served as both a linker and blocking agent to the sensing platform (Fig. 15a–c). For all measurements, selectivity of the sensing platform was confirmed by injecting non-target biomolecules to the active region prior to target injection. The LOD for E103, an antibody that specifically recognizes U1A, is approximately 1 nM, which is comparable to fluorescence-based detection with LOD of ~2.3 nM (Chen et al. 2003).

Single-stranded DNA (ssDNA) binding and subsequent formation of double-stranded DNA (dsDNA) was evaluated on SWCNT network and non-passivated Au surfaces. XPS, fluorescent, and QCM studies revealed that efficient DNA hybridization occurs on the Au electrodes at the metal-tube contact, while little or no hybridization can be observed on the semiconducting SWCNT channel. The junction modulation effect was suggested to be the dominating mechanism for DNA detection with CNT–LGFET (Tang et al. 2006). In a separate study using theoretical modeling, ssDNA was found to interact favorably with SWCNT by wrapping around the tubes (Dovbeshko et al. 2003). The conclusion from both experimental and

simulation studies suggests that the strong interaction of ssDNA receptor with the SWCNT is the main reason impeding the subsequent DNA hybridization process, which needs to be taken into consideration for future design of CNTFET-based DNA genosensors.

For immunology applications, the sensing capability of 5 ng/ml PSA detection, with possible detection limit up to 250 pg/ml was demonstrated through a direct antibody–antigen detection methodology (Li et al. 2005). Same detection scheme was adopted in another recent study to compare the performance of aligned array versus nanonet structure. It was concluded in the study that dense, aligned nanonets leads to improve sensitivity which was attributed to the minimal tube-to-tube contact resistance (Palaniappan et al. 2010). Examples of other immuno-complexes tested include 2,4-dichlorophenoxy acetic acid (2, 4-D) for herbicide detection, and 6-monoacetylmorphine, a morphine metabolite (Tey et al. 2010; Wijaya et al. 2010b). Using a competitive assay methodology, a 500 fM detection limit was obtained for 2,4-D detection in soil extract, as shown in Fig. 20b, c (Wijaya et al. 2010b).

4.4 Amplification schemes

In order to achieve lower detection limits, amplification strategies are often introduced to the sensing system. For DNA sensing, the use of divalent cations were shown to promote hybridization efficiency by screening the charge repulsion between DNA strands (Star et al. 2006). In addition, increasing the junction area of a Schottky contact has also been demonstrated to enhance the signal by 10^4 fold improvement, with a detection limit of 1 pM for rabbit Immunoglobulin G (IgG) in 10 mM PBS buffer solution (pH 7.4) (Byon and Choi 2006). The wide-tapered Au–CNT is thought to accommodate more receptor moieties.

As mentioned in Sect. 3, another route for signal enhancement is through pulse gating, where a larger operating window and higher I_{DS} level are obtained. Figure 21a shows the marked difference between the conventional DC sweep versus pulse-gate measurement. Both studies gave a shift toward negative gate bias upon PLL attachment onto the CNT nanonet, which was deduced to be the electrostatic gating effect induced by the positively charged PLL. The shift in threshold voltage was observed to be more prominent in pulse-gated measurements. In addition, the presence of I_{sat} level decreased at high $|V_G|$ regions. This phenomenon was attributed to be a capacitance effect, where an additional dielectric layer of lower dielectric constant than electrolyte solution was generated from the highly packed PLL binding, leading to diminution of I_{sat}. Such observation could only be obtained at high bias region from pulse-gate measurement, but not under conventional DC sweep measurement (Fig. 21b, c) (Wijaya et al. 2010a).

Au nanoparticles have been widely used in electrochemical-based biosensing as labels for molecule

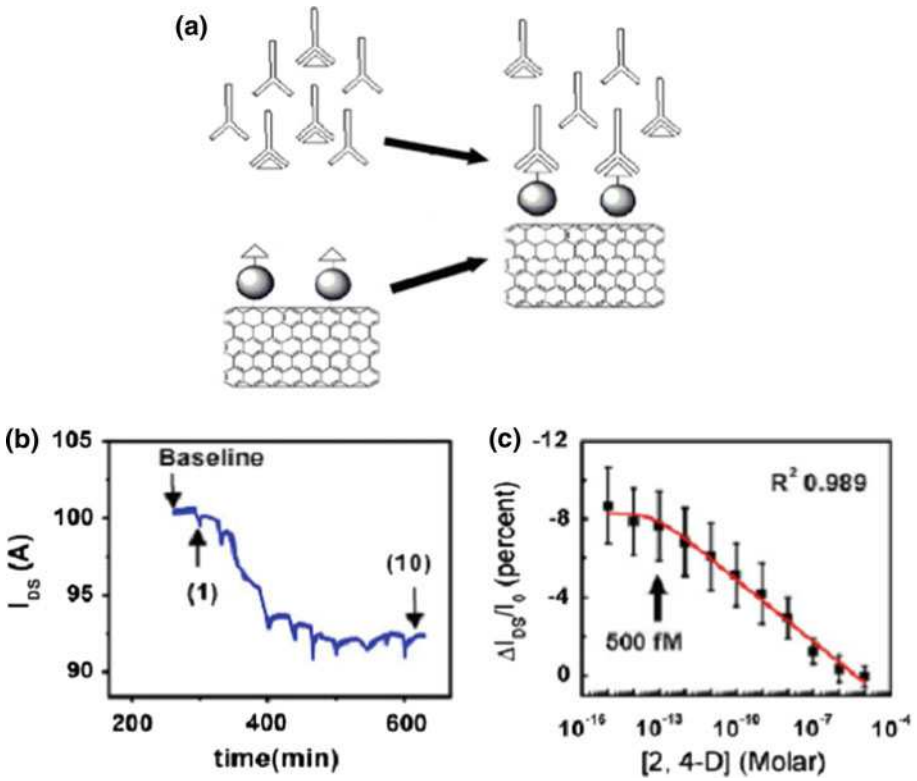

Fig. 20 **a** Schematic of competitive assay protocol. In this protocol, free 2,4-D molecules are pre-mixed with a fixed concentration of corresponding antibody solution to allow the formation of antibody–antigen conjugates with free antibodies in excess after incubation process. By detecting the amount of free antibodies through sensing experiment, the initial concentration of the 2,4-D molecules can be back-tracked. **b** Kinetic response from the LGFET upon exposure of free 2,4-D solution in PB buffer of different concentrations from 50 μM to 5 fM. **c** Calibration curve resultant from the immuno-reaction. Inverse relationship between the signal and free 2,4-D concentration can be revealed in the figure (Wijaya et al. 2010b). Reproduced by permission of The Royal Society of Chemistry

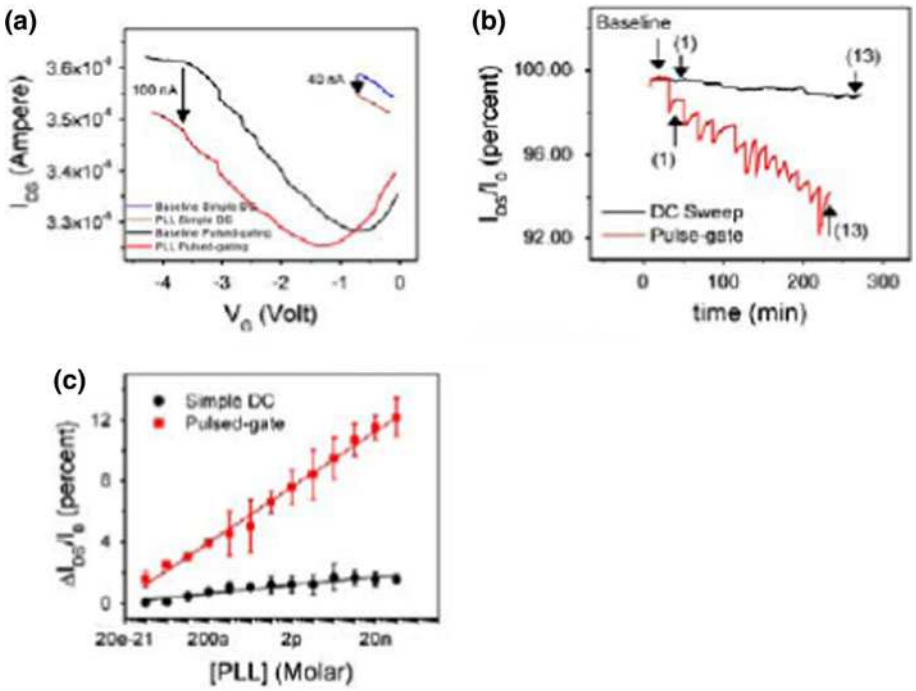

Fig. 21 **a** Comparision of I_{DS}–V_G of conventional DC sweep versus pulse-gate before and after the nanotube exposure toward PLL. The shift obtained from pulse-gate measurement is much larger than in normal DC bias experiment. The kinetic data and the calibration plot in **b** and **c** with concentration tested from 0.2 μM up to 200 nM clearly denotes signal amplification effect and improvement in limit of detection (Wijaya et al. 2010a). Reproduced by permission of The Royal Society of Chemistry

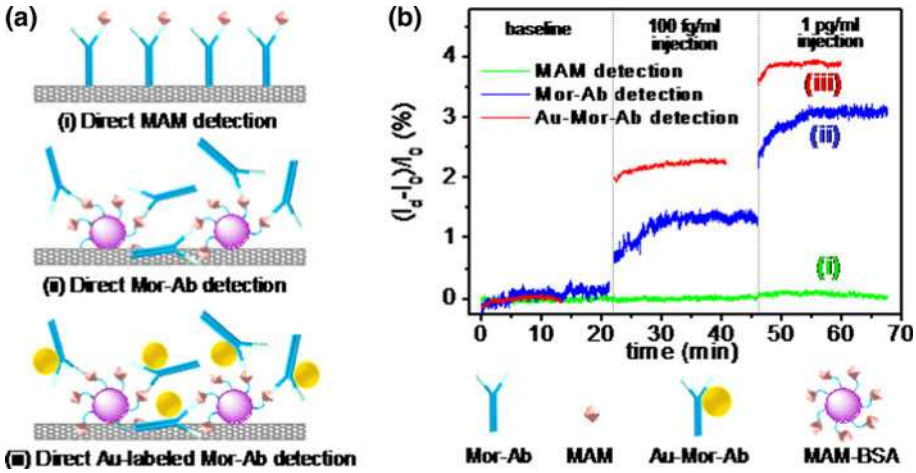

Fig. 22 **a** Three different immuno-complex detection schemes and their corresponding kinetic measurement in **b** to illustrate the signal enhancement effect with Au nanoparticles (Tey et al. 2010). Copyright Wiley-VCH Verlag GmbH & Co KGaA. Reproduced with permission

detection, carriers for other electroactive labels, or signal enhancement tools (Castañeda et al. 2007). Incorporation of Au nanoparticles into CNT–LGFET system has been demonstrated as promising amplification strategy for heroin metabolite detection (Tey et al. 2010). Figure 22a shows the three detection schemes employed in the study and their respective kinetic responses (Fig. 22b). Direct morphine antibody detection, i.e., scheme (ii), brought about an increase in I_{DS} as a result of localized interaction effect from antigen–antibody binding. This conductance increment was further amplified by tagging Au nanoparticles to the morphine antibodies, as shown in scheme (iii) in Fig. 22a. The signal enhancement effect was attributed to the negatively charged Au nanoparticles, which induces positive carriers in the semiconductors, and superimposed on the antibody–antigen interaction, resulting in an overall signal amplification.

5 Future outlook and concluding remarks

We have discussed with examples that CNTs/NWs biosensors in LGFET formats are potential for detection of a broad spectrum of biomolecular interactions and suitable for medical or environmental diagnosis, monitoring, and intervention. The integration of microfluidic technology in the design of the LGFETs brings about advantages, such as: minimal sample volume requirements, short incubation times, and controlled delivery of the sample to the active sensing area. Both NW- and CNT-based sensors show a lot

of promise, and the advantages in nanowire-based sensors include the ability to control the NW properties, growth conditions, top down processing, and the overall in-depth understanding of the microelectronic fabrication processes necessary for sensor fabrication and integration. With improved CNT separation success, processing and purification techniques, CNT-based devices continue to make significant progress while leveraging on its fundamental advantage that all the sensing atoms of Carbon are presented on the surface and are intimately in contact with the interacting biomolecules.

The need for low ionic strength buffer in attaining high sensitivity is a challenge in point-of-care testing of serous fluids and blood serum. This limitation can be overcome by integrating distinct components to the microchips to perform the separation and purification of biomolecules prior to the delivery to CNT/NW channel (Stern et al. 2010). Conjoining biosensors with other microfluidic technologies, such as electrophoresis chromatography (Liu et al. 2008), micro-pump (Ng et al. 2009), micro-mixing (Ng et al. 2008), and opto-electro microfluidics (Jamshidi et al. 2008), will further the realization of lab-on-a-chip device capabilities. The device footprint may be miniaturized toward sub-micrometer-scaled devices which are likely to enable higher sensitivities (Wang et al. 2006). In addition, newer and potentially more sensitive material combinations including graphene (Yan et al. 2007) and organic semiconductors (Torsi 2006; Torsi et al. 2008) could also be incorporated to improve the device sensitivities and stabilities.

From an electronic device perspective, LGFETs may further be integrated with technologies and programming algorithms that would enable truly lab-on-chip operations that would not need semiconductor parameter analyzer type instrumentation for sensing signal transduction (Majewski et al. 2005; Das et al. 2007; Dunn et al. 2006; Wedge et al. 2009; Dost et al. 2007, 2008). Combining a voltage divider/amplifier, and variable gain methods, true lab-on-a-chip operating at low voltages have been reported (Wedge et al. 2009; Dost et al. 2007, 2008). Other approaches that utilize pattern recognition and principal component analysis of an array of sensors is an important component of sensing technologies and has been described elsewhere (Gardner et al. 1992; Fu et al. 2007).

Finally, the possibility to integrate the LGFET with lipid bilayer membranes have also been demonstrated (Artyukhin et al. 2005; Atanasov et al. 2005; Koper 2007; Wallace and Sansom 2009; Thauvin et al. 2008; Zhou et al. 2007; Knoll et al. 2008; Sinner et al. 2009; Misra et al. 2009). A bionanoelectronic device will be the ultimate goal in biosensing to realize the biomimetic e-nose or e-tongue systems which imitate biological systems such as olfactory system (Linda 2005) or taste buds (Prinster et al. 2005) for concurrently detecting and analyzing multiple analytes. Odorant molecules are typically transferred from air to the aqueous environment of the mucosa before binding to olfactory receptors and enabling the sense of smell in humans and animals. Approaches including use of G-protein coupled receptors (GPCRs) (Floriano et al. 2004; Robelek et al. 2007; Leutenegger et al. 2008), ion channels (e.g., Na^+, Ca^{2+}, and Cl^-) (Naumann et al. 2003) that can open and close upon a binding event, would enable monitoring of charge translocation across the membranes integrated with LGFET devices. "Taste" sensors may also be pursued with the LGFET devices since some of the molecules involved in triggering the taste system are highly polar and charged (e.g., amino acids). Biomimetic sensors for smell and taste may therefore be within the realm of possibilities enabled by nanomaterials, biological membranes, and microfluidic-integrated LGFETs.

Acknowledgements The authors would like to thank Professors Bo Liedberg and Wolfgang Knoll for invaluable discussions and inputs on biosensors.

References

Albrecht PM, Lyding JW (2003) Ultrahigh-vacuum scanning tunneling microscopy and spectroscopy of single-walled carbon nanotubes on hydrogen-passivated Si(100) surfaces. Appl Phys Lett 83:5029–5031

Anantram MP, Leonard F (2006) Physics of carbon nanotube electronic devices. Rep Prog Phys 69:507–561

Arnold MS, Stupp SI, Hersam MC (2005) Enrichment of single-walled carbon nanotubes by diameter in density gradients. Nano Lett 5:713–718

Artyukhin AB, Shestakov A, Harper J, Bakajin O, Stroeve P, Noy A (2005) Functional one-dimensional lipid bilayers on carbon nanotube templates. J Am Chem Soc 127:7538–7542

Atanasov V, Knorr N, Duran RS, Ingebrandt S, Offenhausser A, Knoll W, Kopper I (2005) Membrane on a chip: a functional tethered lipid bilayer membrane on silicon oxide surfaces. Biophys J 89:1780–1788

Baker SE, Cai W, Lasseter TL, Weidkamp KP, Hamers RJ (2002) Covalently bonded adducts of deoxyribonucleic acid (DNA) oligonucleotides with single-wall carbon nanotubes: synthesis and hybridization. Nano Lett 2:1413–1417

Bardeen J, Brattain WH (1948) The transistor, a semiconductor triode. Phys Rev 71:230

Baughman RH, Zakhidov AA, de Heer WA (2002) Carbon nanotubes—the route toward applications. Science 297:787–792

Besteman K, Lee J-O, Wiertz FGM, Heering HA, Dekker C (2003) Enzyme-coated carbon nanotubes as single-molecule biosensors. Nano Lett 3:727–730

Boussaad S, Tao NJ, Zhang R, Hopson T, Nagahara LA (2003) In situ detection of cytochrome c adsorption with single walled carbon nanotube device. Chem Commun 1502–1503

Bradley K, Gabriel J-CP, Gruner G (2003) Flexible nanotube electronics. Nano Lett 3:1353–1355

Bradley K, Briman M, Star A, Gruner G (2004) Charge transfer from adsorbed proteins. Nano Lett 4:253–256

Bradley K, Davis A, Gabriel J-CP, Gruner G (2005) Integration of cell membranes and nanotube transistors. Nano Lett 5:841–845

Brady JE, Russell JW, Holum JR (2000) Chemistry: matter and its changes. Wiley, New York

Braun F (1874) Über die Stromleitung durch Schwefelmetalle. Ann Phys Chem 153:56

Brune D, Kim S (1993) Predicting protein diffusion coefficients. PNAS 90:3835–3839

Bunimovich YL, Shin YS, Yeo W-S, Amori M, Kwong G, Heath JR (2006) Quantitative real-time measurements of DNA hybridization with alkylated nonoxidized silicon nanowires in electrolyte solution. J Am Chem Soc 128:16323–16331

Byon HR, Choi HC (2006) Network single-walled carbon nanotube-field effect transistors (SWNT-FETs) with increased Schottky contact area for highly sensitive biosensor applications. J Am Chem Soc 128:2188–2189

Castañeda MT, Alegret S, Merkoçi A (2007) Electrochemical sensing of DNA using gold nanoparticles. Electroanalysis 19:743–753

Chang KS, Chen CC, Sheu JT, Li Y-K (2009) Detection of an uncharged steroid with a silicon nanowire field-effect transistor. Sens Actuators B 138:148–153

Chauhan AK, Aswal DK, Koiry SP, Gupta SK, Yakhmi JV, Sürgers C, Guerin D, Lenfant S, Vuillaume D (2008) Self-assembly of the 3-aminopropyltrimethoxysilane multilayers on Si and hysteretic current–voltage characteristics. Appl Phys A 90:581–589

Chen RJ, Zhang Y, Wang D, Dai H (2001) Noncovalent sidewall functionalization of single-walled carbon nanotubes for protein immobilization. J Am Chem Soc 123:3838–3839

Chen RJ, Bangsaruntip S, Drouvalakis KA, Wong Shi Kam N, Shim M, Li Y, Kim W, Utz PJ, Dai H (2003) Noncovalent functionalization of carbon nanotubes for highly specific electronic biosensors. PNAS 100:4984–4989

Chen RJ, Choi HC, Bangsaruntip S, Yenilmez E, Tang X, Wang Q, Chang Y-L, Dai H (2004) An investigation of the mechanisms of electronic sensing of protein adsorption on carbon nanotube devices. J Am Chem Soc 126:1563–1568

Cherukuri P, Gannon CJ, Leeuw TK, Schmidt HK, Smalley RE, Curley SA, Weisman RB (2006) Mammalian pharmacokinetics of carbon nanotubes using intrinsic near-infrared fluorescence. PNAS 103:18882–18886

Cohen-Karni T, Timko BP, Weiss LE, Lieber CM (2009) Flexible electrical recording from cells using nanowire transistor arrays. PNAS 106:7309–7313

Cui Y, Lieber CM (2001) Functional nanoscale electronic devices assembled using silicon nanowire building blocks. Science 291:851–853

Cui Y, Duan X, Hu J, Lieber CM (2000) Doping and electrical transport in silicon nanowires. J Phys Chem B 104:5213–5216

Cui Y, Wei Q, Park H, Lieber CM (2001) Nanowire nanosensors for highly sensitive and selective detection of biological and chemical species. Science 293:1289–1292

Cui Y, Zhong Z, Wang D, Wang WU, Lieber CM (2003) High performance silicon nanowire field effect transistors. Nano Lett 3:149–152

Curreli M, Li C, Sun Y, Lei B, Gundersen MA, Thompson ME, Zhou C (2005) Selective functionalization of In_2O_3 nanowire mat devices for biosensing applications. J Am Chem Soc 127:6922–6923

Curreli M, Zhang R, Ishikawa FN, Chang H-K, Cote RJ, Zhou C, Thompson ME (2008) Real-time, label-free detection of biological entities using nanowire-based FETs. IEEE Trans Nanotechnol 7:651–667

Das A, Dost R, Richardson T, Grell M, Morrison JJ, Turner ML (2007) A nitrogen dioxide sensor based on an organic transistor constructed from amorphous semiconducting polymers. Adv Mater 19:4018–4023

Dekker C (1999) Carbon nanotubes as molecular quantum wires. Phys Today 52:22–28

Diao P, Liu Z, Wu B, Nan X, Zhang J, Wei Z (2002) Chemically assembled single-wall carbon nanotubes and their electrochemistry. ChemPhysChem 3:898–991

Dillon AC, Gennett T, Jones KM, Alleman JL, Parilla PA, Heben MJ (1999) A simple and complete purification of single-walled carbon nanotube materials. Adv Mater 11:1354–1358

Dong XC, Lau CM, Lohani A, Mhaisalkar SG, Kasim J, Shen ZX, Ho XN, Rogers JA, Li LJ (2008) Electrical detection of femtomolar DNA via gold-nanoparticle enhancement in carbon-nanotube-network field-effect transistors. Adv Mater 20:2389–2393

Dost R, Das A, Grell M (2007) A novel characterization scheme for organic field-effect transistors. J Phys D 40:3563–3566

Dost R, Ray SK, Das A, Grell M (2008) Oscillator circuit based on a single organic transistor. Appl Phys Lett 93:113505

Dovbeshko GI, Repnytska OP, Obraztsova ED, Shtogun YV (2003) DNA interaction with single-walled carbon nanotubes: a SEIRA study. Chem Phys Lett 372:432–437

Dresselhaus MS, Dresselhaus G, Saito R, Jorio A (2005) Raman spectroscopy of carbon nanotubes. Phys Rep 409:47–99

Dunn L, Basu D, Wang L, Dodabalapur A (2006) Organic field effect transistor mobility from transient response analysis. Appl Phys Lett 88:063507

Elfström N, Juhasz R, Sychugov I, Engfeldt T, Karlström AE, Linnros J (2007) Surface charge sensitivity of silicon nanowires: size dependence. Nano Lett 7:2608–2612

Endo M, Strano MS, Ajayan PM (2008) In: Ascheron CE (ed) Carbon nanotubes: advanced topics in the synthesis, structure, properties and applications. Springer, Berlin, pp 13–61

Fan Z, Ho JC, Jacobson ZA, Yerushalmi R, Alley RL, Razavi H, Javey A (2008) Wafer-scale assembly of highly ordered semiconductor nanowire arrays by contact printing. Nano Lett 8:20–25

Floriano WB, Vaidehi N, Goddard WA, II I (2004) Making sense of olfaction through predictions of the 3-D structure and function of olfactory receptors. Chem Senses 29:269–290

Fu J, Li G, Qin Y, Freeman WJ (2007) A pattern recognition method for electronic noses based on an olfactory neural network. Sens Actuators B 125:489–497

Gao Z, Agarwal A, Trigg AD, Singh N, Fang C, Tung C-H, Fan Y, Buddharaju KD, Kong J (2007) Silicon nanowire arrays for label-free detection of DNA. Anal Chem 79:3291–3297

Gao XPA, Zheng G, Lieber CM (2009) Subthreshold regime has the optimal sensitivity for nanowire FET biosensors. Nano Lett 10:547–552

Gao XPA, Zheng G, Lieber CM (2010) Subthreshold regime has the optimal sensitivity for nanowire FET biosensors. Nano Lett 10:547–552

Gardner JW, Shurmer HV, Tan TT (1992) Application of an electronic nose to the discrimination of coffees. Sens Actuators B 6:71–75

Gong K, Yan Y, Zhang M, Su L, Xiong S, Mao L (2005) Electrochemistry and electroanalytical applications of carbon nanotubes: a review. Anal Sci 21:1383–1393

Gooding JJ, Wibowo R, Liu JQ, Yang W, Losic D, Orbons S, Mearns FJ, Shapter JG, Hibbert DB (2003) Protein electrochemistry using aligned carbon nanotube arrays. J Am Chem Soc 125:9006–9007

Gruner G (2006) Carbon nanotube transistors for biosensing applications. Anal Bioanal Chem 384:322–325

Gui E-L, Li L-J, Lee PS, Lohani A, Mhaisalkar SG, Cao Q, Kang SJ, Rogers JA, Tansil NC, Gao Z (2006) Electrical detection of hybridization and threading intercalation of deoxyribonucleic acid using carbon nanotube network field-effect transistors. Appl Phys Lett 89:232104-3

Gui EL, Li L-J, Zhang K, Xu Y, Dong X, Ho X, Lee PS, Kasim J, Shen ZX, Rogers JA, Mhaisalkar SG (2007) DNA sensing by

field-effect transistors based on networks of carbon nanotubes. J Am Chem Soc 129:14427–14432
Guo J, Wang J, Polizzi E, Datta S, Lundstrom M (2003) Electrostatics of nanowire transistors. IEEE Trans Nanotechnol 2:329–334
Hahm J-I, Lieber CM (2004) Direct ultrasensitive electrical detection of DNA and DNA sequence variations using nanowire nanosensors. Nano Lett 4:51–54
Haick H, Hurley PT, Hochbaum AI, Yang P, Lewis NS (2006) Electrical characteristics and chemical stability of non-oxidized, methyl-terminated silicon nanowires. J Am Chem Soc 128:8990–8991
Hazani M, Naaman R, Hennrich F, Kappes MM (2003) Confocal fluorescence Imaging of DNA-functionalized carbon nanotubes. Nano Lett 3:153–155
Heller I, Janssens AM, Mannik J, Minot ED, Lemay SG, Dekker C (2008) Identifying the mechanism of biosensing with carbon nanotube transistors. Nano Lett 8:591–595
Heller I, Mannik J, Lemay SG, Dekker C (2009) Optimizing the signal-to-noise ratio for biosensing with carbon nanotube transistors. Nano Lett 9:377–382
Heo K, Cho E, Yang J-E, Kim M-H, Lee M, Lee BY, Kwon SG, Lee M-S, Jo M-H, Choi H-J, Hyeon T, Hong S (2008) Large-scale assembly of silicon nanowire network-based devices using conventional microfabrication facilities. Nano Lett 8:4523–4527
Hirsch A, Vostrowsky O (2005) Functionalization of carbon nanotubes. In: Schlüter AD (ed) Functional molecular nanostructures. Springer, Berlin, pp 193–237
Hu J, Odom TW, Lieber CM (1999) Chemistry and physics in one dimension: synthesis and properties of nanowires and nanotubes. Acc Chem Res 32:435–445
Huang Y, Duan X, Wei Q, Lieber CM (2001) Directed assembly of one-dimensional nanostructures into functional networks. Science 291:630–633
Huang L, White B, Sfeir MY, Huang M, Huang HX, Wind S, Hone J, O'Brien S (2006) Cobalt ultrathin film catalyzed ethanol chemical vapor deposition of single-walled carbon nanotubes. J Phys Chem B 110:11103–11109
Huang X-J, O'Mahony AM, Compton RG (2009) Microelectrode arrays for electrochemistry: approaches to fabrication. Small 5:776
Hussain MA, Kabir MA, Sood AK (2009) On the cytotoxicity of carbon nanotubes. Curr Sci India 96:664–673
Iijima S (1991) Helical microtubules of graphitic carbon. Nature 354:56
Israelachvili J (1991) Intermolecular and surface forces. Academic Press Limited, London
Jamasb S, Collins S, Smith RL (1998) A physical model for drift in pH ISFETs. Sens Actuators B 49:146–155
Jamshidi A, Pauzauskie PJ, Schuck PJ, Ohta AT, Chiou P-Y, Chou J, Yang P, Wu MC (2008) Dynamic manipulation and separation of individual semiconducting and metallic nanowires. Nat Photonics 2:85–89
Javey A, Nam S, Friedman RS, Yan H, Lieber CM (2007) Layer-by-layer assembly of nanowires for three-dimensional, multifunctional electronics. Nano Lett 7:773–777
Jeon KA, Son HJ, Kim CE, Shon MS, Yoo KH, Choi AM, Jung HI, Lee SY (2006) Biosensor with oxide nanowires. In: 5th IEEE conference on sensors, pp 1265–1268
Jiang K, Schadler LS, Siegel RW, Zhang X, Zhang H, Terrones M (2004) Protein immobilization on carbon nanotubes via a two-step process of diimide-activated amidation. J Mater Chem 14:37–39
Jo G, Maeng J, Kim T-W, Hong W-K, Choi B-S, Lee T (2007) Channel-length and gate-bias dependence of contact resistance and mobility for In_2O_3 nanowire field effect transistors. J Appl Phys 102:084508
Kahng D, Atalla MM (1960) Silicon-silicon dioxide surface device. In: IRE device research conference
Kang SJ, Kocabas C, Kim H-S, Cao Q, Meitl MA, Khang D-Y, Rogers JA (2007a) Printed multilayer superstructures of aligned single-walled carbon nanotubes for electronic applications. Nano Lett 7:3343–3348
Kang SJ, Kocabas C, Ozel T, Shim M, Pimparkar N, Alam MA, Rotkin SV, Rogers JA (2007b) High-performance electronics using dense, perfectly aligned arrays of single-walled carbon nanotubes. Nat Nanotechnol 2:230–236
Kim DR, Zheng X (2008) Numerical characterization and optimization of the microfluidics for nanowire biosensors. Nano Lett 8:3233–3237
Kim W, Choi HC, Shim M, Li Y, Wang D, Dai H (2002) Synthesis of ultralong and high percentage of semiconducting single-walled carbon nanotubes. Nano Lett 2:703–708
Kim Y, Minami N, Zhu W, Kazaoui S, Azumi R, Matsumoto M (2003) Langmuir–Blodgett films of single-wall carbon nanotubes: layer-by-layer deposition and in-plane orientation of tubes. Jpn J Appl Phys 42:7629–7634
Kim A, Ah CS, Yu HY, Yang J-H, Baek I-B, Ahn C-G, Park CW, Jun MS, Lee S (2007a) Ultrasensitive, label-free, and real-time immunodetection using silicon field-effect transistors. Appl Phys Lett 91:103901–103903
Kim SN, Rusling JF, Papadimitrakopoulos F (2007b) Carbon nanotubes for electronic and electrochemical detection of biomolecules. Adv Mater 19:3214–3228
Kim Y-K, Park SJ, Koo JP, Kim GT, Hong S, Ha JS (2007c) Control of adsorption and alignment of V_2O_5 nanowires via chemically functionalized patterns. Nanotechnology 18:015304
Kim JP, Lee BY, Hong S, Sim SJ (2008) Ultrasensitive carbon nanotube-based biosensors using antibody-binding fragments. Anal Biochem 381:193–198
Knoll W, Köper I, Naumann R, Sinner E-K (2008) Tethered bimolecular lipid membranes—a novel model membrane platform. Electrochim Acta 53:6680–6689
Kocabas C, Shim M, Rogers JA (2006) Spatially selective guided growth of high-coverage arrays and random networks of single-walled carbon nanotubes and their integration into electronic devices. J Am Chem Soc 128:4540–4541
Kojima A, Hyon CK, Kamimura T, Maeda M, Matsumoto K (2005) Protein sensor using carbon nanotube field effect transistor. Jpn J Appl Phys 44:1596–1598
Kolasinski KW (2006) Catalytic growth of nanowires: vapor-liquid-solid, vapor-solid-solid, solution-liquid-solid and solid-liquid-solid growth. Curr Opin Solid State Mater 10:182–191
Kong J, Franklin NR, Zhou C, Chapline MG, Peng S, Cho K, Dai H (2000) Nanotube molecular wires as chemical sensors. Science 287:622–625
Koper I (2007) Insulating tethered bilayer lipid membranes to study membrane proteins. Mol Biosyst 3:651–657
Kreupl F, Graham AP, Duesberg GS, Steinhögl W, Liebau M, Unger E, Hönlein W (2002) Carbon nanotubes in interconnect applications. Microelectron Eng 64:399–408
Kumar B, Tan HS, Ramalingam N, Mhaisalkar SG (2009) Integration of ink jet and transfer printing for device fabrication using nanostructured materials. Carbon 47:321–324
Kwang H et al (2009) Massive integration of inorganic nanowire-based structures on solid substrates for device applications. J Mater Chem 19:901
Lacerda L, Bianco A, Prato M, Kostarelos K (2006) Carbon nanotubes as nanomedicines: from toxicology to pharmacology. Adv Drug Deliv Rev 58:1460–1470
Lacerda L, Raffa S, Prato M, Bianco A, Kostarelos K (2007) Cell-penetrating CNTs for delivery of therapeutics. Nano Today 2:38–43
Larrimore L, Nad S, Zhou XJ, Abruna H, McEuen PL (2006) Probing electrostatic potentials in solution with carbon nanotube transistors. Nano Lett 6:1329–1333

Lee M, Im J, Lee BY, Myung S, Kang J, Huang L, Kwon YK, Hong S (2006) Linker-free directed assembly of high-performance integrated devices based on nanotubes and nanowires. Nat Nanotechnol 1:66–71

Lee M, Baik KY, Noah M, Kwon Y-K, Lee J-O, Hong S (2009) Nanowire and nanotube transistors for lab-on-a-chip applications. Lab Chip 9:2267–2280

LeMieux MC, Roberts M, Barman S, Jin YW, Kim JM, Bao Z (2008) Self-sorted, aligned nanotube networks for thin-film transistors. Science 321:101–104

Leutenegger M, Lasser T, Sinner EK, Robelek R (2008) Imaging of G protein-coupled receptors in solid-supported planar lipid membranes. Biointerphases 3:FA136–FA145

Li Y, Kim W, Zhang Y, Rolandi M, Wang D, Dai H (2001) Growth of single-walled carbon nanotubes from discrete catalytic nanoparticles of various sizes. J Phys Chem B 105:11424–11431

Li C, Zhang D, Han S, Liu X, Tang T, Zhou C (2003) Diameter-controlled growth of single-crystalline In_2O_3 nanowires and their electronic properties. Adv Mater 15:143–146

Li C, Curreli M, Lin H, Lei B, Ishikawa FN, Datar R, Cote RJ, Thompson ME, Zhou C (2005) Complementary detection of prostate-specific antigen using In_2O_3 nanowires and carbon nanotubes. J Am Chem Soc 127:12484–12485

Lieber CM, Wang ZL (2007) Functional nanowires. MRS Bull 3:99–108

Lin T-W, Hsieh P-J, Lin C-L, Fang Y-Y, Yang J-X, Tsai C-C, Chiang P-L, Pan C-Y, Chen Y-T (2010) Label-free detection of protein-protein interactions using a calmodulin-modified nanowire transistor. PNAS 107:1047–1052

Linda BB (2005) Unraveling the sense of smell (Nobel Lecture). Angew Chem Int Ed 44:6128–6140

Liu J, Rinzler AG, Dai H, Hafner JH, Bradley RK, Boul PJ, Lu A, Iverson T, Shelimov K, Huffman CB, Rodriguez-Macias F, Shon Y-S, Lee TR, Colbert DT, Smalley RE (1998) Fullerene pipes. Science 280:1253–1256

Liu J, Casavant MJ, Cox M, Walters DA, Boul P, Lu W, Rimberg AJ, Smith KA, Colbert DT, Smalley RE (1999) Controlled deposition of individual single-walled carbon nanotubes on chemically functionalized templates. Chem Phys Lett 303:125–129

Liu J, Yang S, Lee CS, DeVoe DL (2008) Polyacrylamide gel plugs enabling 2-D microfluidic protein separations via isoelectric focusing and multiplexed sodium dodecyl sulfate gel electrophoresis. Electrophoresis 29:2241–2250

Lu W, Lieber CM (2006) Semiconductor nanowires. J Phys D 39:R387–R406

Lu M-P, Hsiao C-Y, Lo P-Y, Wei J-H, Yang Y-S, Chen M-J (2006) Semiconducting single-walled carbon nanotubes exposed to distilled water and aqueous solution: electrical measurement and theoretical calculation. Appl Phys Lett 88:053114-3

Maehashi K, Matsumoto K, Kerman K, Takamura Y, Tamiya E (2004) Ultrasensitive detection of DNA hybridization using carbon nanotube field-effect transistors. Jpn J Appl Phys 43:1558–1560

Maehashi K, Katsura T, Kerman K, Takamura Y, Matsumoto K, Tamiya E (2006) Label-free protein biosensor based on aptamer-modified carbon nanotube field-effect transistors. Anal Chem 79:782–787

Majewski LA, Schroeder R, Grell M (2005) One volt organic transistor. Adv Mater 17:192–196

Martel R, Schmidt T, Shea HR, Hertel T, Avouris P (1998) Single- and multi-wall carbon nanotube field-effect transistors. Appl Phys Lett 73:2447–2449

Martinez MT, Tseng Y-C, Ormategui N, Loinaz I, Eritja R, Bokor J (2009) Label-free DNA biosensors based on functionalized carbon nanotube field effect transistors. Nano Lett 9:530–536

Meitl MA, Zhou Y, Gaur A, Jeon S, Usrey ML, Strano MS, Rogers JA (2004) Solution casting and transfer printing single-walled carbon nanotube films. Nano Lett 4:1643–1647

Melosh NA, Boukai A, Diana F, Gerardot B, Badolato A, Petroff PM, Heath JR (2003) Ultrahigh-density nanowire lattices and circuits. Science 300:112–115

Minot ED, Janssens AM, Heller I, Heering HA, Dekker C, Lemay SG (2007) Carbon nanotube biosensors: the critical role of the reference electrode. Appl Phys Lett 91:093507

Misra N, Martinez JA, Huang S-CJ, Wang Y, Stroeve P, Grigoropoulos CP, Noy A (2009) Bioelectronic silicon nanowire devices using functional membrane proteins. PNAS 106:13780–13784

Nair PR, Alam MA (2007) Design considerations of silicon nanowire biosensors. IEEE Trans Electron Dev 54:3400–3408

Naumann R, Walz D, Schiller SM, Knoll W (2003) Kinetics of valinomycin-mediated K+ ion transport through tethered bilayer lipid membranes. J Electroanal Chem 550–551:241–252

Ng WY, Goh S, Lam YC, Yang C, Rodriguez I (2008) DC-Biased AC-electroosmotic and AC-electrothermal flow mixing in microchannels. Lab Chip 9:802–809

Ng WY, Lam YC, Rodriguez I (2009) Experimental verification of Faradaic charging in ac electrokinetics. Biomicrofluidics 3:022405

Palaniappan A, Goh WH, Tey JN, Wijaya IPM (2010) Aligned carbon nanotubes on quartz substrate for liquid gated biosensing. Biosens Bioelectron 25:1989–1993

Panini NV, Messina GA, Salinas E, Fernandez H, Raba J (2008) Integrated microfluidic systems with an immunosensor modified with carbon nanotubes for detection of prostate specific antigen (PSA) in human serum samples. Biosens Bioelectron 23:1145–1151

Park J-U, Meitl MA, Hur S-H, Usrey ML, Strano MS, Kenis PJA, Rogers JA (2006) In situ deposition and patterning of single-walled carbon nantoubes by laminar flow and controlled flocculation in microfluidic channels. Angew Chem Int Ed 45:581–585

Park J, Shin G, Ha JS (2007) Thickness and density controllable pattern transfer of DODAB/V_2O_5 nanowire hybrid film. Nanotechnology 18:405301

Patolsky F, Zheng G, Hayden O, Lakadamyali M, Zhuang X, Lieber CM (2004) Electrical detection of single viruses. PNAS 101:14017–14022

Patolsky F, Timko BP, Yu G, Fang Y, Greytak AB, Zheng G, Lieber CM (2006a) Detection, stimulation, and inhibition of neuronal signals with high-density nanowire transistor arrays. Science 313:1100–1104

Patolsky F, Zheng G, Lieber CM (2006b) Fabrication of silicon nanowire devices for ultrasensitive, label-free, real-time detection of biological and chemical species. Nat Protoc 1:1711–1724

Patolsky F, Zheng G, Lieber CM (2006c) Nanowire-based biosensor. Anal Chem 4261–4269

Peng H, Alemany LB, Margrave JL, Khabashesku VN (2003) Sidewall carboxylic acid functionalization of single-walled carbon nanotubes. J Am Chem Soc 125:15174–15182

Poghossian A, Cherstvy A, Ingebrandt S, Offenhausser A, Schoning MJ (2005) Possibilities and limitations of label-free detection of DNA hybridization with field-effect-based devices. Sens Actuators B 111–112:470–480

Polizu S, Savadogo O, Poulin P, Yahia L (2006) Applications of carbon nanotubes-based biomaterials in biomedical nanotechnology. J Nanosci Nanotechnol 6:1883–1904

Popov AM, Lozovik YE, Fiorito S, Yahia L (2007) Biocompatibility and applications of carbon nanotubes in medical nano robots. Int J Nanomed 2:361–372

Prinster SC, Hague C, Hall RA (2005) Heterodimerization of G protein-coupled receptors: specificity and functional significance. Pharmacol Rev 57:289–298

Pui T-S, Agarwal A, Ye F, Balasubramanian N, Chen P (2009) CMOS-compatible nanowire sensor arrays for detection of cellular bioelectricity. Small 5:208–212

Robelek R, Lemker ES, Wiltschi B, Kirste V, Naumann R, Oesterhelt D, Sinner EK (2007) Incorporation of in vitro synthesized GPCR into a tethered artificial lipid membrane system. Angew Chem Int Ed 46:605–608

Rosenblatt S, Yaish Y, Park J, Gore J, Sazonova V, McEuen PL (2002) High performance electrolyte gated carbon nanotube transistors. Nano Lett 2:869–872

Rudikoff S, Potter M (1976) Size differences among immunoglobulin heavy chains from phosphorylcholine-binding proteins. PNAS 73:2109–2112

Sheehan PE, Whitman LJ (2005) Detection limits for nanoscale biosensors. Nano Lett 5:803–807

Sinner EK, Ritz S, Naumann R, Schiller S, Knoll W (2009) Advances in clinical chemistry. Elsevier Academic Press Inc, San Diego, pp 159–179

So H-M, Won K, Kim YH, Kim B-K, Ryu BH, Na PS, Kim H, Lee J-O (2005) Single-walled carbon nanotube biosensors using aptamers as molecular recognition elements. J Am Chem Soc 127:11906–11907

Star A, Gabriel J-CP, Bradley K, Gruner G (2003) Electronic detection of specific protein binding using nanotube FET devices. Nano Lett 3:459–463

Star A, Tu E, Niemann J, Gabriel JCP, Joiner CS, Valcke C (2006) Label-free detection of DNA hybridization using carbon nanotube network field-effect transistors. PNAS 103:921–926

Stéphane C, Moreno M, Maurizio P (2007) Separation of metallic and semiconducting single-walled carbon nanotubes via covalent functionalization. Small 3:1672–1676

Stern E, Klemic JF, Routenberg DA, Wyrembak PN, Turner-Evans DB, Hamilton AD, LaVan DA, Fahmy TM, Reed MA (2007a) Label-free immunodetection with CMOS-compatible semiconducting nanowires. Nature 445:519–522

Stern E, Wagner R, Sigworth FJ, Breaker R, Fahmy TM, Reed MA (2007b) Importance of the Debye screening length on nanowire field effect transistor sensors. Nano Lett 7:3405–3409

Stern E, Vacic A, Rajan NK, Criscione JM, Park J, Ilic BR, Mooney DJ, Reed MA, Fahmy TM (2010) Label-free biomarker detection from whole blood. Nat Nanotechnol 5:138–142

Strano MS, Dyke CA, Usrey ML, Barone PW, Allen MJ, Shan H, Kittrell C, Hauge RH, Tour JM, Smalley RE (2003) Electronic structure control of single-walled carbon nanotube functionalization. Science 301:1519–1522

Streifer JA, Kim H, Nichols BM, Hamers RJ (2005) Covalent functionalization and biomolecular recognition properties of DNA-modified silicon nanowires. Nanotechnology 16:1868–1873

Strother T, Hamers RJ, Smith LM (2000) Covalent attachment of oligodeoxyribonucleotides to amine-modified Si (001) surfaces. Nucleic Acids Res 28:3535–3541

Sun C, Mathews N, Zheng M, Sow CH, Wong LH, Mhaisalkar SG (2010) Aligned tin oxide nanonets for high-performance transistors. J Phys Chem C 114:1331–1336

Tang X, Bansaruntip S, Nakayama N, Yenilmez E, Chang Y-l, Wang Q (2006) Carbon nanotube DNA sensor and sensing mechanism. Nano Lett 6:1632–1636

Teillaud JL, Desaymard C, Giusti AM, Haseltine B, Pollock RR, Yelton DE, Zack DJ, Scharff MD (1983) Monoclonal antibodies reveal the structural basis of antibody diversity. Science 222:721–726

Tey JN, Wijaya IPM, Wang Z, Goh WH, Palaniappan A, Mhaisalkar SG, Rodriguez I, Dunham S, Rogers JA (2009) Laminated, microfluidic-integrated carbon nanotube based biosensors. Appl Phys Lett 94:013107

Tey JN, Gandhi S, Wijaya IPM, Palaniappan A, Wei J, Rodriguez I, Suri CR, Mhaisalkar SG (2010) direct detection of heroin metabolites using a carbon nanotubes liquid gated field effect transistor based competitive immunoassay. Small doi:10.1002/smll.200902139

Thauvin C, Rickling S, Schultz P, Celia H, Meunier S, Mioskowski C (2008) Carbon nanotubes as templates for polymerized lipid assemblies. Nat Nanotechnol 3:743–748

Timko BP, Cohen-Karni T, Yu G, Qing Q, Tian B, Lieber CM (2009) Electrical recording from hearts with flexible nanowire device arrays. Nano Lett 9:914–918

Torsi L (2006) Organic thin-film transistors as analytical and bioanalytical sensors. Anal Bioanal Chem 384:309

Torsi L, Farinola GM, Marinelli F, Tanese MC, Omar OH, Valli L, Babudri F, Palmisano F, Zambonin PG, Naso F (2008) A sensitivity-enhanced field-effect chiral sensor. Nat Mater 7:412–417

Viswanathan S, Rani C, Anand AV, Ho JA (2009) Disposable electrochemical immunosensor for carcinoembryonic antigen using ferrocene liposomes and MWCNT screen-printed electrode. Biosens Bioelectron 24:1984–1989

Wallace EJ, Sansom MSP (2009) Carbon nanotube self-assembly with lipids and detergent: a molecular dynamics study. Nanotechnology 20:045101

Wang J (2002) Analytical electrochemistry. Wiley-VCH, New Mexico

Wang J, Liu G, Jan MR (2004) Ultrasensitive electrical biosensing of proteins and DNA: carbon-nanotube derived amplification of the recognition and transduction events. J Am Chem Soc 126:3010–3011

Wang WU, Chen C, Lin K-H, Fang Y, Lieber CM (2005) Label-free detection of small-molecule-protein interactions by using nanowire nanosensors. PNAS 102:3208–3212

Wang L, Fine D, Sharma D, Torsi L, Dodabalapur A (2006) Nanoscale organic and polymeric field-effect transistors as chemical sensors. Anal Bioanal Chem 384:310–321

Wang C-W, Pan C-Y, Wu H-C, Shih P-Y, Tsai C-C, Liao K-T, Lu L-L, Hsieh W-H, Chen C-D, Chen Y-T (2007) In situ detection of Chromogranin A released from living neurons with a single-walled carbon-nanotube field-effect transistor. Small 3:1350–1355

Wedge DC, Das A, Dost R, Kettle J, Madec M-B, Morrison JJ, Grell M, Kell DB, Richardson TH, Yeates S, Turner ML (2009) Real-time vapour sensing using an OFET-based electronic nose and genetic programming. Sens Actuators B 143:365–372

Whang D, Jin S, Wu Y, Lieber CM (2003) Large-scale hierarchical organization of nanowire arrays for integrated nanosystems. Nano Lett 3:1255–1259

Wijaya IPM, Rodriguez I, Mhaisalkar SG (2008) Effect of alignment on the temperature-resistance response of dielectrophoretically assembled multiwalled carbon nanotube films. Int J Nanosci 7:199–205

Wijaya IPM, Gandhi S, Nie TJ, Wangoo N, Rodriguez I, Shekhawat G, Suri CR, Mhaisalkar SG (2009) Protein/carbon nanotubes interaction: the effect of carboxylic groups on conformational and conductance changes. Appl Phys Lett 95:073704

Wijaya IPM, Tey JN, Palaniappan A, Rodriguez I, Mhaisalkar SG (2010a) Investigation of sensing mechanism and signal amplification in carbon nanotube based microfluidic liquid-gated transistors via pulsating gate bias. Lab Chip. doi:10.1039/B2926631C

Wijaya IPM, Tey JN, Gandhi S, Boro R, Palaniappan A, Goh WH, Rodriguez I, Suri CR, Mhaisalkar SG (2010b) Femto molar detection of 2, 4-dichlorophenoxyacetic acid herbicides via competitive immunoassays using microfluidic based carbon nanotube liquid gated transistor. Lab Chip 10:634–638

Yan YH, Li S, Shen LQ, Chan-Park MB, Zhang Q (2006) Large-scale submicron horizontally aligned single-walled carbon nanotube surface arrays on various substrates produced by a fluidic assembly method. Nanotechnology 17:5696–5701

Yan Q, Huang B, Yu J, Zheng F, Zang J, Wu J, Gu B-L, Liu F, Duan W (2007) Intrinsic current-voltage characteristics of graphene nanoribbon transistors and effect of edge doping. Nano Lett 7:1469–1473

Yao D, Zhang G, Li B (2008) A universal expression of band gap for silicon nanowires of different cross-section geometries. Nano Lett 8:4557–4561

Yu X, Munge B, Patel V, Jensen G, Bhirde A, Gong JD, Kim SN, Gillespie J, Gutkind JS, Papadimitrakopoulos F, Rusling JF (2006) Carbon nanotube amplification strategies for highly sensitive immunodetection of cancer biomarkers. J Am Chem Soc 128:11199–11205

Yun Y, Dong Z, shanov VN, Schulz MJ (2007) Electrochemical impedance measurement of prostate cancer cells using carbon nanotube array electrodes in a microfluidic channel. Nanotechnology 18:465505

Zhang Y-B, Kanungo M, Ho AJ, Freimuth P, van der Lelie D, Chen M, Khamis SM, Datta SS, Johnson ATC, Misewich JA, Wong SS (2007) Functionalized carbon nanotubes for detecting viral proteins. Nano Lett 7:3086–3091

Zhang F, Ulrich B, Reddy RK, Venkatraman VL, Prasad S, Vu TQ, Hsu S-T (2008a) Fabrication of submicron IrO_2 nanowire array biosensor platform by conventional complementary metal-oxide-semiconductor process. Jpn J Appl Phys 47:1147–1151

Zhang G-J, Chua JH, Chee R-E, Agarwal A, Wong SM, Buddharaju KD, Balasubramanian N (2008b) Highly sensitive measurements of PNA-DNA hybridization using oxide-etched silicon nanowire biosensors. Biosens Bioelectron 23:1701–1707

Zheng G, Patolsky F, Cui Y, Wang WU, Lieber CM (2005) Multiplexed electrical detection of cancer markers with nanowire sensor arrays. Nat Biotechnol 23:1294–1301

Zhou Y, Hu L, Gruner G (2006) A method of printing carbon nanotube thin films. Appl Phys Lett 88:123109

Zhou X, Moran-Mirabal JM, Craighead HG, McEuen PL (2007) Supported lipid bilayer/carbon nanotube hybrids. Nat Nanotechnol 2:185–190